https://doi.org/10.5194/egusphere-2026-4054
Preprint. Discussion started: 15 July 2026

A GOSAT-Based Assessment of Interannual Variability in Terrestrial CO_2 Fluxes and Its Hydroclimatic Drivers

Sanam N. Vardag[1,2], Sourish Basu[3,4], André Butz[1,2,5], Eva-Marie Metz[6]

[1]Institute of Environmental Physics, Heidelberg University, Heidelberg, 69120, Germany
[2]Heidelberg Center for the Environment, Heidelberg University, Heidelberg, 69120, Germany
[3]Goddard Space Flight Center, NASA, Greenbelt, Maryland, USA
[4]Earth System Science Interdisciplinary Center, University of Maryland, College Park, Maryland, USA
[5]Interdisciplinary Center for Scientific Computing, Heidelberg University, Heidelberg, Germany
[6]Division of Geological and Planetary Sciences, California Institute of Technology, Pasadena, California, USA

Correspondence to: Sanam N. Vardag (Sanam.vardag@uni-heidelberg.de)

Abstract. Understanding interannual variability (IAV) in terrestrial CO_2 fluxes is essential for constraining ecosystem responses to climatic anomalies and future carbon-climate feedbacks. A 14-year GOSAT record spanning 2009 to end of 2022 now enables a robust global assessment of regional IAV. Here, we analyse annual net land CO_2 fluxes from nine in situ-constrained inversions and three GOSAT-based inversions, and compare them with the TRENDY v13 ensemble mean of dynamic global vegetation models (DGVMs). We find that DGVMs show weaker IAV than the inversion-based flux estimates in almost all regions. In Australia, boreal and temperate North America, and Eurasian Temperate, differences in NEE anomalies between GOSAT-based inversions and TRENDY are strongly related to hydroclimatic anomalies, with soil moisture and temperature emerging as dominant drivers in different regions. These results suggest that DGVMs underestimate the sensitivity of NEE to climate variability in key regions. The extended satellite record makes it possible to use the hydroclimatic anomalies of the last 14 years to identify deficiencies in ecosystem parameterizations and thereby reduce uncertainty in the global carbon budget.

1 Introduction

The annual growth rate of atmospheric CO_2 exhibits substantial interannual variability (IAV), which is primarily driven by year-to-year fluctuations in terrestrial land-atmosphere CO_2 exchange (Friedlingstein et al., 2026). These fluctuations arise because the terrestrial carbon cycle is sensitive to climatic variability, including variations in temperature, precipitation, soil moisture, vapour pressure deficit, and large-scale climate modes such as the El Niño–Southern Oscillation (ENSO) (Ahlström et al., 2015; Bastos et al., 2018; Piao et al., 2020; Poulter et al., 2011; Poulter et al., 2014; Wang et al., 2022; Zhang et al., 2018; Jiang et al., 2026). Understanding this IAV is essential to determine how terrestrial ecosystems respond to climatic anomalies and, as a result, how the land carbon sink may evolve under future climate change and disturbances.

https://doi.org/10.5194/egusphere-2026-4054
Preprint. Discussion started: 15 July 2026

Dynamic global vegetation models (DGVMs) provide a process-based framework for simulating terrestrial carbon fluxes and their response to climatic variability and long-term climate change (Sitch et al., 2015; Sitch et al., 2024). However, the simulated net CO_2 exchange depends strongly on model structure, process representation, and parameter choices. Different models include different formulations of photosynthesis, respiration, allocation, phenology, disturbances, and land-use processes. Previous studies have shown that DGVMs often differ substantially in simulated net fluxes and their variability, and that their representation of climate sensitivity remains uncertain (Foster et al., 2024; Teckentrup et al., 2021; Padrón et al., 2022; Vardag et al., 2025).

Atmospheric inverse modelling provides an independent, top-down estimate of surface CO_2 fluxes by optimizing fluxes such that simulated atmospheric CO_2 concentrations agree with observations within uncertainties. Traditionally, such inversions have relied on in situ CO_2 measurements. These measurements are highly precise and provide long time series, but their spatial coverage is limited, especially in remote and sparsely monitored regions. As a result, in situ-only inversions are often insufficient to robustly constrain regional carbon fluxes over large parts of the globe (Chen et al., 2021; Jung et al., 2020; Villalobos et al., 2020; Metz et al., 2025).

Satellite observations of column-averaged dry-air mole fractions of CO_2, hereafter XCO_2, provide complementary information by sampling broad spatial regions, including areas with sparse in situ coverage. By adding observations over remote land regions, satellite XCO_2 measurements can improve constraints on regional carbon fluxes and thereby help diagnose ecosystem responses to climatic variability (Byrne et al., 2020; Palmer et al., 2019; Sellers et al., 2018; Villalobos et al., 2020; Vardag et al., 2025; Metz et al., 2025, 2024). Previous work has demonstrated that assimilating satellite observations can reveal carbon-cycle dynamics that are difficult to infer from in situ observations alone. For example, (Metz et al., 2023) showed that satellite-constrained inversions provide key information on the carbon-cycle dynamics of Australia and reveal processes that are not detected by in situ-only inversions.

Here, we use a 14-year record of GOSAT XCO_2 observations together with in situ CO_2 measurements in the TM5-4DVAR inversion system to assess terrestrial carbon-cycle variability from 2009 to 2022. We compare the resulting top-down flux estimates with in situ-only inversions and with process-based estimates from DGVMs, which were collected within the TRENDYv13 ensemble (Sitch et al., 2024; Friedlingstein et al., 2025). In addition to quantifying the magnitude of regional IAV, we investigate whether mismatches between data-constrained inversions and DGVMs are systematically related to hydroclimatic variability. We analyse IAV across different regions and assess whether differences between GOSAT-based inversions and DGVMs can be explained by differing sensitivities to hydroclimatic drivers.

Specifically, we address the following questions:

(1) What are the magnitude and spatial pattern of IAV in continental-scale terrestrial CO_2 exchange over 2009–2022?
(2) How do these estimates differ between priors, in situ-only inversions, GOSAT-based inversions, and DGVMs?
(3) What causes mismatches between inversions and DGVMs and can mismatches be related to hydroclimatic variability in some regions?

https://doi.org/10.5194/egusphere-2026-4054
Preprint. Discussion started: 15 July 2026

2. Methods

2.1 Study regions

We analyse terrestrial CO_2 flux variability at the scale of the TRANSCOM-3 land regions (Gurney et al., 2004). The TRANSCOM regions represent broad continental and climatic zones and have been widely used in global carbon-cycle inversion studies. All gridded flux products are aggregated to annual totals for each TRANSCOM land region.

2.2 Top-down inversion estimates

In total, we analyse nine in situ-based inversion products and three GOSAT-based inversion products. Eight of the in situ-only inversions and two of the GOSAT-based inversions are taken from the Global Carbon Budget inversion ensemble and are explained in (van der Woude et al., 2025) and shortly introduced in Sect.2.2.1.. We additionally analyse TM5-4DVAR in situ-only and TM5-4DVAR GOSAT+in situ, described in Sect. 2.2.2, thereby contributing a new inversion product based on the well-established Tracer Model 5 four-dimensional variational inversion (TM5-4DVAR) system. Across the three GOSAT-based inversion products analysed here, the satellite constraint is provided by three different GOSAT XCO_2 retrieval algorithms, namely NIES (Yoshida et al., 2013), ACOS (O'Dell et al., 2012), and RemoTeC (Butz, 2024; Butz et al., 2011). All inversion products are listed in Table A1. We remove fire emissions to obtain fire-corrected net biome productivity (NBP) comparable to the DGVM-based estimates (Sect. 2.3). All flux fields are regridded to 1° × 1° before applying the TRANSCOM region mask.

2.2.1 GCP inversions

We use global top-down CO_2 flux inversions from (Luijkx et al., 2025), which have been further described in (van der Woude et al., 2025). From this ensemble, we select all eight in situ-only inversions and two GOSAT-based inversions, CMS-Flux and NTFVAR, that assimilate GOSAT together with in situ observations. CMS-Flux additionally assimilates OCO-2 XCO_2 since 2014. The NBP fluxes contain the sum of the natural land sink and the fire and land-use change emissions. Fire emissions from GFEDv5 (van der Werf et al., 2025) are subtracted to be compatible to DGVM estimates.

2.2.2 TM5-4DVAR inversion

We use the TM5-4DVAR, to infer surface CO_2 fluxes from atmospheric CO_2 observations (Basu et al., 2013). We perform two main inversion configurations. The first assimilates only in situ CO_2 observations, while the second assimilates GOSAT XCO_2 retrievals using RemoteCv2.4.1 (Butz, 2024) in addition to in situ CO_2 observations. The in situ observations are taken from the CO_2 GLOBALVIEWplus ObsPack version GV+9.1 and ObsPack NRT 9.2, which provides a collection of atmospheric CO_2 mole-fraction measurements from global monitoring sites.

https://doi.org/10.5194/egusphere-2026-4054
Preprint. Discussion started: 15 July 2026

TM5-4DVAR optimizes weekly biosphere and ocean fluxes on a regular 3° longitude × 2° latitude global grid. Prior biosphere fluxes are prescribed from the Carnegie–Ames–Stanford Approach (CASA) biogeochemical model (van der Werf et al., 2017). These priors are based on climatological mean fluxes and therefore impose a strictly repeating seasonal cycle with no IAV. Fossil-fuel emissions and fire emissions are prescribed. Fossil-fuel emissions are taken from the Open-source Data Inventory for Anthropogenic CO_2, and fire emissions are prescribed from the Quick Fire Emissions Dataset using a climatological seasonal cycle such that the total prior land flux has no imposed IAV. To obtain fire-corrected terrestrial NBP comparable to the DGVM-based estimates, we add the internal QFED fire flux back to the optimized terrestrial flux and subtract the GFEDv5 fire emissions.

2.3 Dynamic global vegetation models

To assess the process-based representation of carbon-cycle variability, we use the TRENDY v13 ensemble of DGVMs (Sitch et al., 2024), also used in (Friedlingstein et al., 2025). Specifically, we analyse the S3 simulations, in which models are forced by time-varying atmospheric CO_2, climate, and land-use information. TRENDY models simulate terrestrial vegetation dynamics, photosynthesis, respiration, carbon allocation, turnover, disturbance, and land-use processes, although the exact representation of these processes differs among models (Sitch et al., 2024).

We use monthly output from 21 DGVMs listed in Table A2. The available flux components differ between models; therefore, the construction of fire-corrected net land-atmosphere CO_2 exchange depends on the provided variables. For comparison with the top-down inversion estimates, we focus on fire-corrected land–atmosphere CO_2 exchange and apply a consistent sign convention, with positive fluxes denoting net CO_2 release to the atmosphere and negative fluxes denoting net CO_2 uptake by the land. Where NBP and fire emissions are available, we derive fire-corrected NBP. Where NBP is not available, we calculate the same quantity from the gross flux components as

$$\mathrm{NBP} - \mathrm{fFIRE} = \mathrm{TER} - \mathrm{GPP} + \mathrm{fLUC} = (R_a + R_h) - \mathrm{GPP} + \mathrm{fLUC}, \tag{1}$$

where R_a and R_h are autotrophic and heterotrophic respiration, respectively, TER denotes terrestrial ecosystem respiration and fLUC denotes the fluxes from land-use change. In fLUC is not provided, we calculate NBP-fire using equation (1), but neglecting fLUC. An overview of model-specific flux construction is given in Table A2. In the following, for simplicity, we refer to this fire-corrected net land-atmosphere CO_2 exchange as NEE. Riverine and other lateral carbon fluxes are not added explicitly, because most DGVMs are internally mass-conserving and adding external lateral-flux estimates could lead to double counting. Although lateral carbon exports may be substantial in the mean, their IAV is comparatively small relative to the variability analysed here (e.g. (Ciais et al., 2026). The ensemble mean is calculated from all 21 models after applying the harmonized sign convention and flux definition.

2.4 Interannual variability metric and annual anomalies

https://doi.org/10.5194/egusphere-2026-4054
Preprint. Discussion started: 15 July 2026

We quantify IAV using the standard deviation of annual regional flux totals over the analysis period. For each product and region, monthly fluxes are first aggregated to annual totals (Jan–Dec). The IAV is then calculated as the standard deviation of the annual flux totals over the common period 2009–2022 for the GOSAT-based and in situ-only TM5 inversions, and over the corresponding available period for each comparison product. The annual NEE anomalies are derived by subtracting the mean NEE value from the period 2009 to 2022 from the annual NEE for each individual product and region.

2.5 Hydroclimatic drivers and anomaly calculation

To investigate the climatic drivers of regional carbon-flux variability, we use temperature, precipitation, and soil-moisture fields from the ERA5-Land reanalysis (Muñoz-Sabater et al., 2021). ERA5-Land provides monthly meteorological and hydrological variables on a 0.25° × 0.25° grid. We use 2 m air temperature and upper-layer soil moisture at 0–7 cm depth. These variables are selected because they have been identified as key drivers of photosynthesis, respiration, and NEE (Yun et al., 2025). All ERA5-Land fields are aggregated to the same TRANSCOM regions as the flux products. Annual hydroclimatic and NEE anomalies are derived by subtracting the mean value from 2009 to 2022, respectively.

2.6 Multilinear regression analysis

To quantify the relationship between carbon-flux anomalies and hydroclimatic anomalies, we fit a multilinear regression model for each region and flux product, as well as for the difference between the inversion flux products and the DGVMs. The annual NEE anomaly (NEE') is modelled as a linear function of anomalies in temperature (T') and soil moisture (SM'):

$$\mathrm{NEE}' = \beta_0 + \beta_T T' + \beta_{SM} SM' + \epsilon \quad (2)$$

Here, β_0 is the intercept, β_T and β_{SM} are the regression coefficients, and ϵ is the residual term.

This linear formulation is used as a first-order diagnostic of annual hydroclimatic sensitivity. Because ecosystem responses to hydroclimatic variability can in reality be nonlinear and state-dependent, the fitted relationships should not be interpreted as a process description. We therefore restrict discussion in Sect. 3.2 to regions where the fit satisfies predefined goodness-of-fit and significance criteria described below.

We assess in which regions the differences between anomalies from the inversions and the DGVMs are significantly related to hydroclimatic variability using the coefficient of determination (R^2) and the p-value of the overall F-test, which tests whether the full regression model explains significantly more variance than an intercept-only model. Only regions satisfying both the $R^2 > 0.4$ criterion and the significance threshold of $p < 0.05$ are considered in the subsequent analysis in Sect. 3.2.

For regions showing significant hydroclimatic sensitivity, we then compare the responses of the different data sets to temperature and soil-moisture variability. The p-values of the individual predictors are used to assess whether a given predictor contributes significantly to the fit after accounting for the other predictor.

https://doi.org/10.5194/egusphere-2026-4054
Preprint. Discussion started: 15 July 2026

Because temperature and soil-moisture anomalies are often correlated, especially during drought or wet years, we analyse partial sensitivities rather than independent causal effects. We therefore also examine correlations among the predictors to identify regions where collinearity may influence the attribution of carbon-flux variability to individual drivers.

3. Results

3.1 Robustness of the data sets

The GOSAT record covers 14 years over 2009–2022 and spans a wide range of climatic anomalies. This is important because IAV estimates based on short time periods can be biased by the occurrence of specific climatic conditions included in the record. Figure A1 shows the mean absolute bias introduced when IAV is estimated from shorter time windows relative to the full 14-year period. Although the sensitivity to record length is region dependent, the bias generally decreases with increasing window length and becomes flatter after approximately 11 years. This suggests that the current record length is in a regime where regional IAV estimates are substantially more robust than estimates based on the shorter satellite records available previously. This now puts us in the position to analyse the IAV and the climate sensitivity of the regional carbon fluxes based on the GOSAT XCO_2 time series.

In addition to the record length, the robustness of regional IAV estimates is affected by structural uncertainty within both top-down inversions and DGVMs. Atmospheric inversions can differ because of transport errors, prior flux assumptions, observation selection, and inversion setup; these uncertainties generally become more important at smaller spatial scales, where transport representation and sparse observational coverage exert a stronger influence on the inferred fluxes (Zhang et al., 2023). We therefore focus on relatively large TransCom regions, for which aggregation reduces some of the sensitivity to local transport and representation errors. To further limit dependence on any single inversion system, we compare multiple data-driven products and interpret the GOSAT-constrained results in the context of the broader inversion ensemble. Similarly, we use the TRENDY multi-model ensemble rather than relying on individual DGVMs, following common practice in carbon-cycle assessments such as the Global Carbon Budget.

3.2 Spatial patterns of interannual variability

Figure 1 shows the spatial distribution of IAV in annual terrestrial CO_2 fluxes across TRANSCOM regions. The prior biosphere fluxes exhibit the lowest IAV, with regional IAV values of typically around 50 TgC yr^{-1}. Both, the in situ only inversion and the GOSAT-based inversion show larger IAV than the prior, indicating that the enhanced IAV in the posterior estimates is not inherited from the prior, but is introduced through the atmospheric observational constraint. Because all products analysed here are expressed as fire-corrected NBP (hereafter NEE; see Sect. 2.3), the product differences are not simply caused by fire emissions. However, fire is treated differently in the inversions and DGVMs, so uncertainty in the IAV of fire emissions could still affect the inferred product mismatch. We therefore show in Figure A2the regional IAV of GFED fire emissions and their relative contribution to the total regional flux IAV. Fire-emission variability is regionally heterogeneous and contributes substantially in some regions, especially in Eurasia Boreal (78 %) and Tropical Asia (44 %), while being much smaller in most

https://doi.org/10.5194/egusphere-2026-4054
Preprint. Discussion started: 15 July 2026

other regions (see Fig. A2). This suggests that uncertainty in the representation of fire does not explain the overall enhancement of IAV in the inversions across all regions.

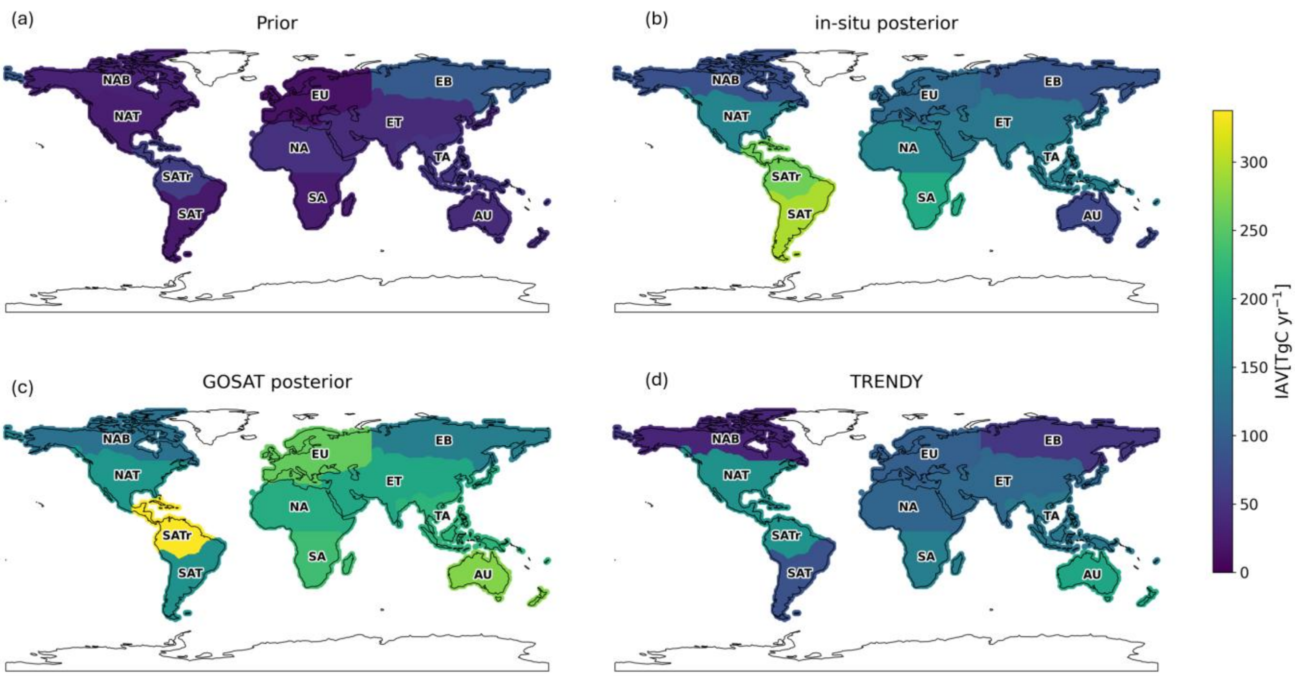

Figure 1: Prior and posterior estimates of regional NEE IAV. Maps show the IAV of annual NEE for TRANSCOM regions over 2009–2022. The upper-left panel shows the mean prior IAV, calculated from the TM5-4DVAR prior and all GCP prior ensemble members. The upper-right and lower-left panels show posterior IAV for the in situ group and the GOSAT-based group, respectively, using the corresponding ensemble-mean monthly flux time series. The lower-right panel shows the IAV of the TRENDY ensemble-mean NEE time series. All fluxes are expressed in TgC yr^{-1}.

For the in situ-only inversion averaged across TRANSCOM regions, IAV increases from roughly 50 TgC yr^{-1} in the prior to about 100 TgC yr^{-1} in the in situ-only inversion, corresponding to an increase by a factor of 2, but with strong regional differences. A larger IAV is particularly visible in South American Tropical, South American Temperate, and Southern Africa, where the in situ-only ensemble-mean IAV increases roughly by a factor of 4.

The GOSAT-based inversion shows substantially larger IAV in several continental regions. The strongest increases relative to the in situ-only inversion occur in Australia, Europe, Eurasia, and South American Tropical, with regional IAV increasing by a factor of roughly 4 in Australia, Eurasia and Europe, and by a factor of roughly 6 in South American Tropical. This suggests that the additional spatial coverage provided by XCO_2 observations, in addition to in situ observations, may allow the inversion to resolve stronger year-to-year variations in terrestrial CO_2 exchange than can be inferred from the in situ network alone.

The TRENDY ensemble mean generally exhibits substantially weaker IAV than the GOSAT-based inversion in all regions. It is also lower than the in situ-only inversion in most regions, but not in North American Temperate and Australia. Averaged across TRANSCOM regions, the TRENDY ensemble-mean IAV is approximately 30% lower than the GOSAT-based inversions, but large regional differences occur.

One possible explanation for a smaller IAV in the TRENDY ensemble mean is the averaging over many different DGVMs. If individual models differ in the phase and amplitude of interannual anomalies, the multi-model mean will dampen part of the variability. Figure A3 compares the IAV of the TRENDY ensemble mean with the IAV of individual TRENDY models for each TRANSCOM region. In most regions, individual TRENDY models (as well as individual in-situ and GOSAT inversions) span a wide range of IAV values, while the TRENDY ensemble mean lies toward the lower end of this distribution. Several individual models show larger IAV than the ensemble mean, confirming that ensemble averaging reduces IAV when model anomalies are not fully coherent. However, this averaging effect alone does not explain the discrepancy relative to the inversions. The average IAV of the individual TRENDY models is still generally lower than the IAV inferred by the atmospheric inversions, particularly for the GOSAT-based inversions. This indicates that the lower variability of the TRENDY ensemble mean also reflects an underestimation of IAV in the DGVMs themselves.

We further analyse reasons for the discrepancy of IAV in DGVMs and inversions by analysing the mean seasonal cycle and its variability. We find that across regions and flux products, IAV generally increases with the amplitude of the mean seasonal cycle (Fig. A4a), but this relationship shows substantial scatter. By contrast, IAV correlates even stronger to the standard deviation of yearly seasonal-cycle amplitude (Fig. A4b), suggesting that stronger interannual modulation of the seasonal cycle is more closely linked to IAV than the mean seasonal-cycle amplitude alone.

A comparison of annual anomaly correlations and relative IAV with respect to the GOSAT-based product shows that the mismatch differs between product families (Fig. A5). In many regions, the in situ-only product remains moderately correlated with the GOSAT-based annual anomalies but exhibits weaker variability, indicating that it captures part of the year-to-year dynamics while underestimating their amplitude. By contrast, the TRENDY ensemble mean often shows both reduced variability and weaker correlation, suggesting that the mismatch is not only a damping of IAV, but in several regions also a weaker reproduction of the year-to-year anomaly structure (Fig. A5).

Finally, we analyse how the products differ in their sensitivity to hydroclimatic variability. Since the 2009–2022 period includes pronounced climatic anomalies, including wet and dry extremes in several semi-arid and tropical regions, the higher IAV in the GOSAT-based inversion may indicate that atmospheric observations capture stronger ecosystem responses to hydroclimatic forcing than represented in the TRENDY ensemble mean. We therefore hypothesize that the IAV of the TRENDY model mean is underestimated because the models either underestimate the magnitude of the flux response to climate

https://doi.org/10.5194/egusphere-2026-4054
Preprint. Discussion started: 15 July 2026

anomalies, differ in the timing of that response, or both. In the next section, we therefore examine whether differing sensitivities to hydroclimatic anomalies can explain the differences in IAV across products.

3.3 Hydroclimatic controls on regional NEE anomalies

We conduct a multi-linear regression analysis on the difference in annual NEE anomalies between the inversions and the TRENDY ensemble mean with respect to soil-moisture and temperature anomalies, to determine whether hydroclimatic anomalies can explain the mismatch in IAV between data products. Since the atmospheric inversions infer flux anomalies from CO_2 observations and are agnostic to soil-moisture or temperature variability, a significant relationship with these anomalies would indicate that the inversion-TRENDY mismatch is climate dependent. Such a result would suggest that hydroclimatic drivers govern NEE variability differently in the observation-constrained estimates than represented by the TRENDY ensemble mean. The multilinear regression analysis reveals that the relationship between NEE anomalies and hydroclimatic drivers differs strongly among regions. In some regions, NEE anomalies are strongly associated with soil-moisture or temperature anomalies, while in others the explained variance is small. Fig. 2 shows the overall R^2 of the multilinear fit for all regions, as well as the individual p-values.

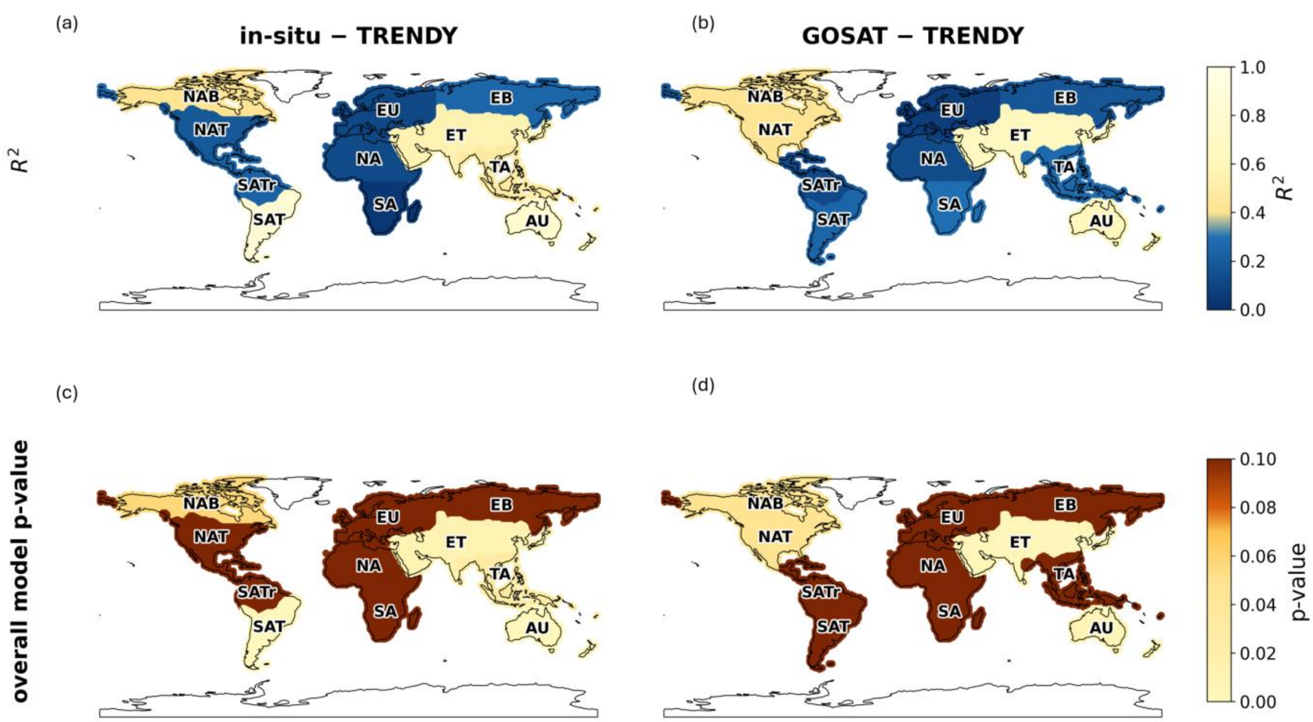

https://doi.org/10.5194/egusphere-2026-4054
Preprint. Discussion started: 15 July 2026

Fig. 2: Statistics overview for the multi-linear fit. Overview over R^2 (a,b) and p-values (c,d) for the differences of the NEE anomalies between in-situ and TRENDY models (a,c) and GOSAT and TRENDY models (b,d). The color bar was chosen to have strong gradients at the thresholds we use for determining that differences systematically vary with climate anomalies.

Applying a $p < 0.05$ threshold together with an $R^2 > 0.4$ criterion, we identify the regions of Australia, North America Boreal, North America Temperate, and Eurasian Temperate as regions in which the differences in NEE anomalies between the GOSAT-based and DGVM-based flux estimates are structured by hydroclimatic variability. In these regions, the GOSAT-based fluxes also show larger IAV than the TRENDY ensemble mean, suggesting that differences in hydroclimatic sensitivity contribute to the mismatch. As fire is already accounted for in both the inversion-based and DGVM-based products through the fire-corrected flux definition, any remaining influence can only arise from differences on how fire is represented. Fig. A2 shows that the relative fire contribution is small in North America Temperate (8 %) and Eurasian Temperate (6 %), moderate in Australia (19 %), and larger in North America Boreal (31 %). This suggests that uncertainty in fire variability may contribute to the boreal signal, but is unlikely to be the dominant explanation for the mismatch overall.

We present the time series of NEE, soil moisture, and temperature anomalies together with fitted regression relationships and partial-regression diagnostics (Fig. 3) and discuss the main drivers per region (Sect. 3.3.1–3.3.4 and Figs. A6-A9). As additional robustness tests, we repeated the analysis excluding 2009, which is only partially covered by GOSAT observations, and we compared the GOSAT-based product not only to the TRENDY ensemble mean but also to the five TRENDY models with the lowest monthly RMSE relative to GOSAT. Excluding 2009 leads to only minor changes in the anomaly statistics and does not affect the main conclusions for any of the selected regions, while the annual anomalies of the five selected TRENDY models remain similar to the TRENDY ensemble mean and the mismatch to the GOSAT-based estimate persists in the key regions (Fig. A10). This suggests that the discrepancy is not confined to poorly performing models, but also characterizes a subset of TRENDY models that already reproduce the monthly GOSAT variability comparatively well.

https://doi.org/10.5194/egusphere-2026-4054
Preprint. Discussion started: 15 July 2026

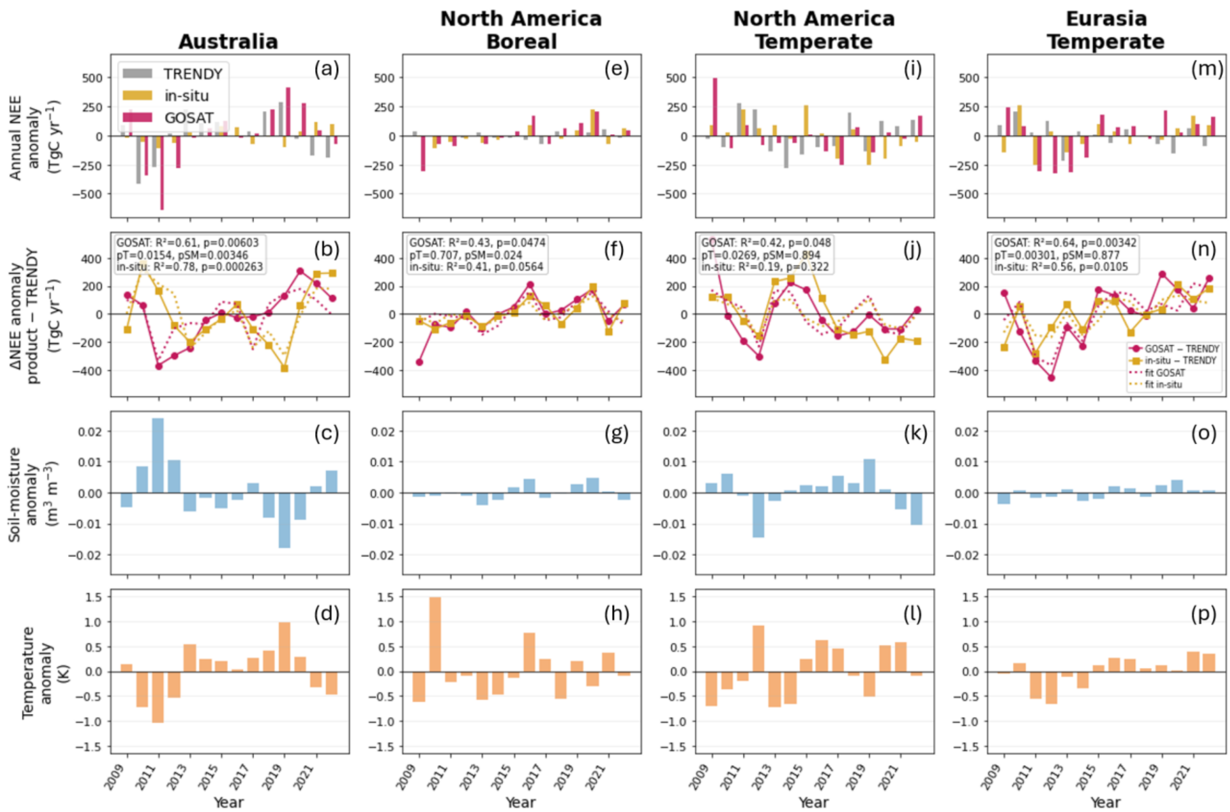

Figure 3: NEE anomaly (a,e,f,m), difference in NEE anomaly to TRENDY (b,f,j,n), soil moisture anomaly (c,g,h,o) and temperature anomaly (d,h,l,p) for the regions of Australia, North American Boreal, North American temperate and Eurasian Temperate. The difference in the NEE anomalies are fitted using Eq (2).

3.3.1 Australia

Australian NEE anomalies in both the TRENDY ensemble mean and the GOSAT-based flux inversion show pronounced ENSO-related variability, with enhanced uptake during wet La Niña periods, most prominently in 2010–2012 and again during the recent 2020–2022 multi-year La Niña, and reduced uptake or net carbon release during dry, warm El Niño or drought–fire periods such as 2015/16 and 2019/20. The in situ-constrained fluxes show much weaker IAV and remain closer to the prior, consistent with the limited observational constraint provided by the sparse in situ network in this region (Metz et al., 2023). Both TRENDY and the GOSAT-based inversion show a strong coupling between Australian NEE anomalies and hydroclimatic variability. A multilinear regression using temperature and soil-moisture anomalies explains a large fraction of the NEE anomaly variability in both TRENDY ($R^2 = 0.83$) and GOSAT ($R^2 = 0.90$) (Fig. A6). However, the magnitude of NEE anomalies is smaller in TRENDY than in GOSAT, indicating that the TRENDY ensemble mean underestimates the amplitude of the Australian carbon-cycle response to wet and dry extremes.

https://doi.org/10.5194/egusphere-2026-4054
Preprint. Discussion started: 15 July 2026

More specifically, in the GOSAT-based regression, NEE decreases with increasing soil-moisture anomalies, indicating enhanced net CO_2 uptake, or reduced net CO_2 release, under wetter conditions. By contrast, TRENDY mean shows a positive NEE–soil-moisture sensitivity (see Fig. A6), implying larger net CO_2 release when soils are wetter. The attribution to individual drivers is complicated by the strong correlation between temperature and soil-moisture anomalies, particularly during droughts, when warm anomalies often coincide with dry soils. Nevertheless, the opposite sign of the soil-moisture sensitivity suggests that TRENDY mean does not only underestimate the magnitude of the hydroclimatic response in Australia, but may also misrepresent the direction of the net ecosystem response to soil-moisture anomalies.

The high explained variance of the fit throughout the analysed period indicates that Australian NEE anomalies can be understood to a large extent from observed temperature and soil-moisture variability. The post-2019 decrease in NEE is therefore broadly consistent with the transition from El Niño-related dry conditions toward wetter La Niña conditions. However, recent flood-related dryland CO_2 emissions (Eyre et al., 2026) and reported changes in Australian tropical forest carbon storage (Carle et al., 2025) may additionally affect post-2019 carbon-cycle variability. Within the annual regression framework used here, we find no evidence for an exceptional change in hydroclimatic sensitivity over the analysed period.

3.3.2. North America Boreal

North America Boreal (NAB) shows weaker overall NEE anomaly variability than Australia, but the inversions still indicate a clear sensitivity to hydroclimatic variability. Both, the in situ-constrained and GOSAT-based inversions show a larger IAV than the TRENDY model mean. Differences between inversions and DGVM correlate significantly. A multilinear regression of the individual NEE anomalies with temperature and soil-moisture anomalies explain a substantial fraction of the annual NEE anomaly variability ($R^2 = 0.58, p = 0.008$ for in situ; $R^2 = 0.47, p = 0.031$ for GOSAT; Fig. A7).

The partial regression analysis suggests that this sensitivity is dominated primarily by soil moisture rather than temperature. Both inversion products show a strong positive soil-moisture sensitivity, whereas the temperature effect is weak in GOSAT and moderately negative in the in situ inversion. In contrast to Australia, temperature and soil-moisture anomalies are only moderately correlated ($r = 0.27$), making the regression more informative for separating individual drivers. TRENDY, in contrast, shows only very weak sensitivities to both predictors. A plausible interpretation is that hydrological controls on boreal carbon exchange are too weak in the TRENDY ensemble mean compared to what is indicated by the inversions.

3.3.3. North America Temperate

In North America Temperate (NAT), the relationship between annual NEE anomalies and hydroclimatic variability is weaker for the individual flux products than in NAB or Australia. Nevertheless, the GOSAT–TRENDY NEE anomaly difference is significantly explained by temperature and soil-moisture anomalies ($R^2 = 0.42, p = 0.048$), indicating that hydroclimatic variability accounts for a significant part of the mismatch between the inversion and DGVM estimates. In contrast to Australia, temperature and soil-moisture anomalies are only weakly correlated in NAT, which allows a clearer separation of the two

https://doi.org/10.5194/egusphere-2026-4054
Preprint. Discussion started: 15 July 2026

drivers. While the fitted sensitivities of the individual products to temperature and soil-moisture anomalies are not significant on their own, the in situ and GOSAT products consistently show a negative temperature sensitivity, whereas TRENDY shows a positive one (Fig. A8). The significant regression of the GOSAT–TRENDY anomaly difference is consistent with this contrast and suggests that the enhanced IAV in the inversions arises from a different temperature response than represented in the TRENDY ensemble mean.

3.3.4. Eurasian Temperate

In Eurasian Temperate (ET), both the in situ-based and GOSAT-based products show a trend in annual NEE anomalies that is much less apparent in the TRENDY ensemble mean. The corresponding data–model anomaly difference therefore also exhibits a trend, which covaries with the concurrent increase in temperature over the analysis period. A multilinear regression using temperature and soil-moisture anomalies explains a large fraction of the GOSAT–TRENDY NEE anomaly difference (R^2 = 0.64), and the in situ–TRENDY difference shows a similar behaviour (R^2 = 0.56).

In contrast to Australia, temperature and soil-moisture anomalies are less correlated in ET, so the regression allows a clearer separation of their contributions. The fitted relationship is dominated by temperature (see Fig. A10), while the contribution from soil moisture is smaller, suggesting that the stronger IAV inferred from the inversions in ET is mainly associated with a stronger temperature sensitivity than represented by the TRENDY ensemble mean. Note, that the individual GOSAT-based inversions show considerable spread in their IAV over ET (see Fig. A3), indicating that the magnitude of the inferred variability differs across inversion systems. Nevertheless, the similar behaviour and large IAV of the in situ-based products supports the interpretation that the product mismatch is not altered by biases in satellite data.

At the same time, the interpretation remains less direct than in Australia because the data-driven products show an overall trend in NEE. Part of the fitted temperature relationship may therefore reflect the co-occurrence of longer-term changes rather than purely interannual sensitivity. Nevertheless, the agreement between the GOSAT and in situ ensemble means, and their contrast with TRENDY, indicates that differing temperature sensitivities likely contribute substantially to the product mismatch in ET.

4. Discussion

4.1 GOSAT-based inversions reveal stronger regional interannual variability

The continuous GOSAT record from 2009 to 2022, spanning 14 full years, provides a robust basis for assessing regional IAV because it samples multiple phases of climate variability and reduces the influence of individual extreme years. Its extended temporal coverage allows new insight into continental-scale IAV and into differences between inversions and DGVMs.

We find that the stronger IAV in the GOSAT-based products is not inherited from the climatological prior, but emerges from the observational constraint. Relative to both the prior and the TRENDY ensemble mean, the GOSAT-based inversions therefore indicate a larger amplitude of regional year-to-year carbon-cycle variability. In many regions, the GOSAT-based products also show stronger IAV than the corresponding in situ-only inversions, leveraging the additional satellite XCO_2

https://doi.org/10.5194/egusphere-2026-4054
Preprint. Discussion started: 15 July 2026

observations where the surface network is sparse. Previous studies have shown that satellite XCO_2 observations can reduce regional flux uncertainty and reveal variability that is only weakly constrained by surface observations alone, particularly over remote continental regions (Wang et al., 2022; Villalobos et al., 2020).

Part of the enhanced variability in the inversions could in principle reflect inversion-specific biases due to transport or observation errors as differences in transport and inversion setup are known to contribute to spread in top-down flux estimates (Basu et al., 2018). However, the fact that stronger IAV appears in several independent GOSAT-based products using different GOSAT XCO_2 retrievals and different transport models, and that these products remain broadly consistent with the in situ-based inversions while extending their variability in sparsely observed regions, suggests that such effects are unlikely to be the only explanation for the regional pattern of enhanced variability found here.

The TRENDY ensemble mean generally shows weaker IAV than the GOSAT-based inversion products. While ensemble averaging reduces the variability of the multi-model mean, this is not the dominant explanation for the mismatch, because in many regions the individual DGVMs also tend to show smaller IAV than the inversion flux products, particularly than the GOSAT-constrained inversions. Across products, IAV is only loosely related to the amplitude of the mean seasonal cycle, but more tightly related to the year-to-year variability of seasonal-cycle amplitude (Fig. A4), suggesting that stronger interannual modulation of the seasonal cycle is more closely linked to IAV than the mean seasonal-cycle amplitude alone.

A comparison of annual anomaly correlations and relative variability with respect to the GOSAT-based product (Fig. A5) indicates that the data–model mismatch often involves not only weaker anomaly amplitude, but also structural differences in the year-to-year anomaly pattern. In several regions, including North America Boreal, South American Tropical, and Eurasian Temperate, the TRENDY ensemble mean shows both reduced variability and low correlation with the GOSAT-based anomalies. This points to structural differences that cannot be resolved by amplitude scaling alone, because the mismatch involves not only the size of the anomalies but also their temporal sequence from year to year. The discrepancy between DGVMs and the GOSAT-based product therefore often reflects both damped IAV and a weaker reproduction of interannual anomaly dynamics.

The comparatively low IAV of the TRENDY ensemble mean is consistent with earlier evidence that terrestrial ecosystem models often underestimate carbon-cycle variability. (Lin et al., 2023) showed that models substantially underestimate GPP IAV relative to eddy-covariance and observation-based estimates, especially in water-limited ecosystems, while (MacBean et al., 2021) found that DGVMs underestimate dryland net CO_2 flux variability, largely because of insufficient GPP sensitivity to water availability. These studies therefore indicate, from a flux-tower perspective, that DGVMs may dampen ecosystem responses to hydroclimatic variability, particularly in drylands and water-limited systems. Our analysis supports this finding by showing that a similar underrepresentation of variability emerges when DGVMs are evaluated against an independent atmospheric constraint from GOSAT-based top-down NEE estimates.

https://doi.org/10.5194/egusphere-2026-4054
Preprint. Discussion started: 15 July 2026

4.2 Regional mismatches point to differing hydroclimatic sensitivities

Hydroclimatic sensitivity has previously been identified as an important source of mismatch between DGVMs and atmospheric inversions. (Bastos et al., 2020) showed that disagreement in NBP IAV explains a large fraction of global and regional bottom-up versus top-down differences, and attributed part of this mismatch to differing responses to climate variability. (Wang et al., 2022) and (Padrón et al., 2022) showed that DGVMs still show substantial uncertainty in their hydroclimatic sensitivities. We find that in several regions the mismatch between GOSAT-based and DGVM-based anomaly time series is itself significantly related to hydroclimatic variability, with DGVMs showing weaker sensitivities than data-driven flux products. This indicates that weaker IAV in DGVMs likely reflects not only differences in seasonal amplitude, but also differences in climate sensitivity. This interpretation is also supported when restricting the comparison to the five TRENDY models with the lowest monthly RMSE relative to GOSAT-based estimates, the structure of the mean of the 5 best models remains similar to the full TRENDY ensemble mean and still differs systematically from the GOSAT-based estimate (Fig. A10).

In this sense, our results confirm the broader conclusion of (Bastos et al., 2020) that differences in IAV are a key contributor to bottom-up versus top-down mismatch, while pointing to a different sign and magnitude of hydroclimatic sensitivity in the more recent, satellite-constrained data sets analysed here.

Australia provides the clearest example of a climatically structured mismatch. The strong hydroclimatic control seen in both TRENDY and the GOSAT-based inversion, combined with the much smaller anomaly amplitude in TRENDY, indicates that the models capture part of the climate response but underestimate its magnitude. More importantly, the fitted sensitivities differ qualitatively: the GOSAT-based inversion shows a much stronger negative sensitivity to soil-moisture anomalies, whereas TRENDY does not reproduce this behaviour. This points to a process-level deficiency in TRENDY ensemble mean. A likely explanation is that the GOSAT-based product captures soil-respiration pulses following rewetting, consistent with the Birch effect interpretation of (Metz et al., 2023) whereas this mechanism is too weak or absent in the TRENDY ensemble mean. In the recent post-2019 period, the sensitivity of NEE anomalies to hydroclimatic drivers remain largely consistent with hydroclimatic forcing despite possible additional effects from additional disturbances such as floodings (Eyre et al., 2026). Our regression results do not indicate an exceptional change in large-scale hydroclimatic sensitivity during this period. Australia therefore provides a particularly strong example that the multilinear regression, despite its simplicity, can reveal physically meaningful processes and help identify specific shortcomings in the model representation of hydroclimatic sensitivity.

Uncertainty in boreal carbon fluxes of the high northern latitudes remains high and process-based models do not fully capture the timing and magnitude of carbon exchange inferred from atmospheric constraints (Wen et al., 2026). For NAB, we find that data-driven products indicate a substantially stronger sensitivity to soil-moisture variability than the TRENDY ensemble mean. Both the GOSAT-based and in situ inversions show a clear annual moisture response, whereas TRENDY remains much weaker, suggesting that the ensemble mean underrepresents the role of moisture anomalies in shaping NEE variability in this

https://doi.org/10.5194/egusphere-2026-4054
Preprint. Discussion started: 15 July 2026

region. Unlike in Australia, this does not point primarily to rewetting pulses, but more generally to a weaker annual moisture sensitivity in the models.

Even over North American Temperate, where observational constraints are comparatively dense, disagreement between top-down and bottom-up NEE estimates remains substantial, supporting findings by (Foster et al., 2024). We find that while annual regressions of the individual products are relatively weak, the GOSAT–TRENDY anomaly difference is significantly related to hydroclimatic variability, in particular to temperature sensitivity. This suggests that, over 2009-2022 the mismatch between inversions and DGVM-based fluxes reflects differing temperature responses. The importance of temperature-sensitivity for interannual variability of terrestrial carbon uptake outside strongly arid systems was recently also reported by (Jiang et al., 2026). This is also the case for Eurasian Temperate, where both the in situ-based and GOSAT-based products show a trend in annual NEE anomalies that is much less apparent in the TRENDY ensemble mean. As a result, the data-model anomaly difference itself also shows a trend, which is correlated with the concurrent increase in temperature over the analysis period. This points to the possibility that the DGVM ensemble mean underestimates the sensitivity of regional carbon exchange to temperature anomalies, in line with previous evidence that large-scale Asian terrestrial carbon fluxes are responsive to climatic variability (Zhang et al., 2014; Jiang et al., 2026). At the same time, this interpretation is not unique. Recent work has also shown that DGVMs underestimate the northern carbon sink because key disturbance-related processes, including fire emissions and especially forest regrowth, are not fully captured (O'Sullivan et al., 2024), which could likewise contribute to the correlation with time.

The regional results indicate that the mismatch between DGVMs and inversion fluxes is systematically related to hydroclimatic variability in many key regions. At the same time, the absence of a strong annual relationship in other regions does not imply the absence of hydroclimatic control. Annual aggregation can mask compensating seasonal responses, and the limited length of the record reduces the power to resolve weaker or nonlinear sensitivities. Our use of a simple linear model and strict fit criteria is therefore intentionally conservative: it likely misses some real hydroclimatic effects, but reduces the risk of overfitting and overinterpreting weak annual relationships.

5. Conclusions

Using the 2009–2022 GOSAT record, we find that continental-scale IAV in terrestrial CO_2 fluxes is generally higher in global inversions than in DGVMs. In several regions, the mismatch between GOSAT-based and DGVM-based anomaly time series is significantly related to hydroclimatic variability, indicating that differences in sensitivity to soil moisture or temperature contribute to the weaker variability of DGVMs. Long-term satellite XCO_2 records therefore provide an important tool for evaluating the magnitude and the climatic drivers of terrestrial carbon-cycle variability.

https://doi.org/10.5194/egusphere-2026-4054
Preprint. Discussion started: 15 July 2026

Appendix A

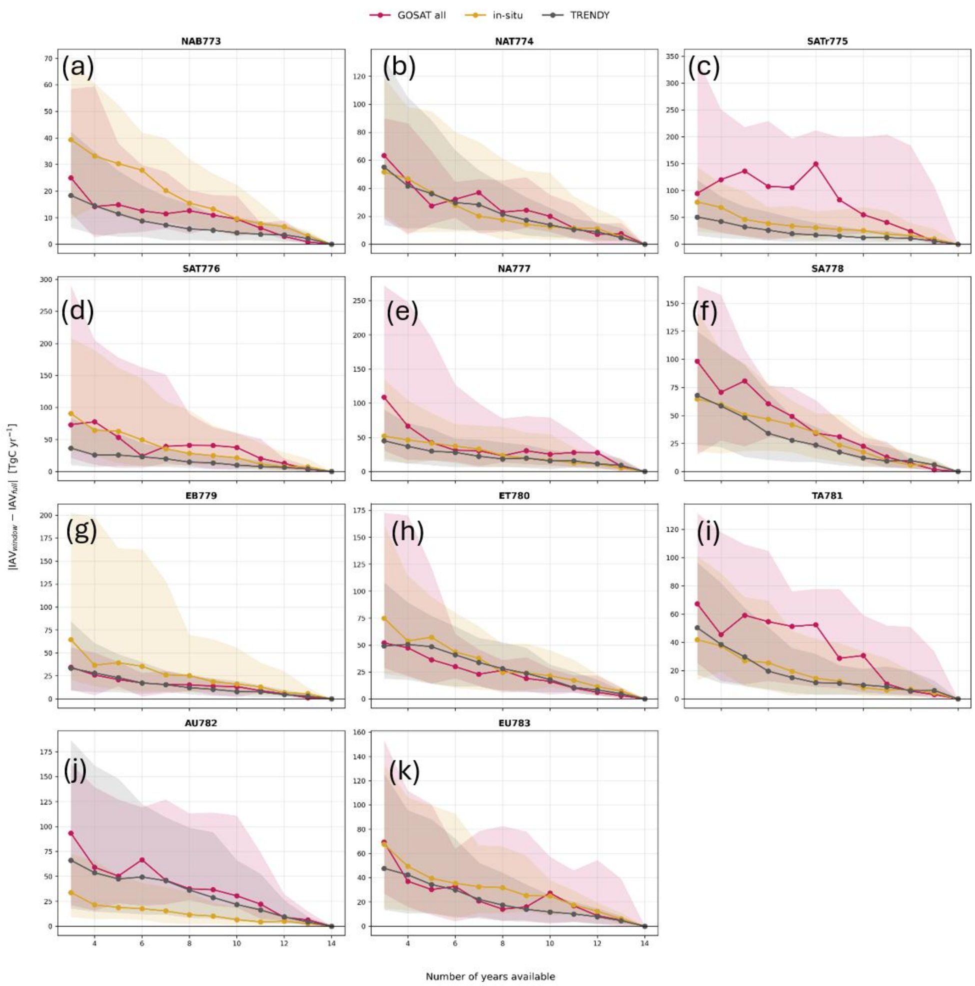

Fig. A1: Absolute difference of IAV based on the time period used (x-axis), and based on the data product (colors). For each TransCom region, the figure shows how estimates of IAV in annual NEE depend on the length of the available observational record. IAV is calculated as the standard deviation of annual NEE totals over all possible consecutive windows of a given length and compared to the IAV derived from the full reference period. Lines show the median absolute difference between the window-based IAV and the full-period IAV, while shaded ranges indicate the spread across individual products or models within each group. Separate colours distinguish the GOSAT-constrained products, in-situ-based products, and TRENDY

https://doi.org/10.5194/egusphere-2026-4054
Preprint. Discussion started: 15 July 2026

models. A decreasing curve indicates that IAV estimates become more stable as the available time series becomes longer; deviations from a smooth decrease indicate that specific years or multi-year events exert a strong influence on the estimated variability.

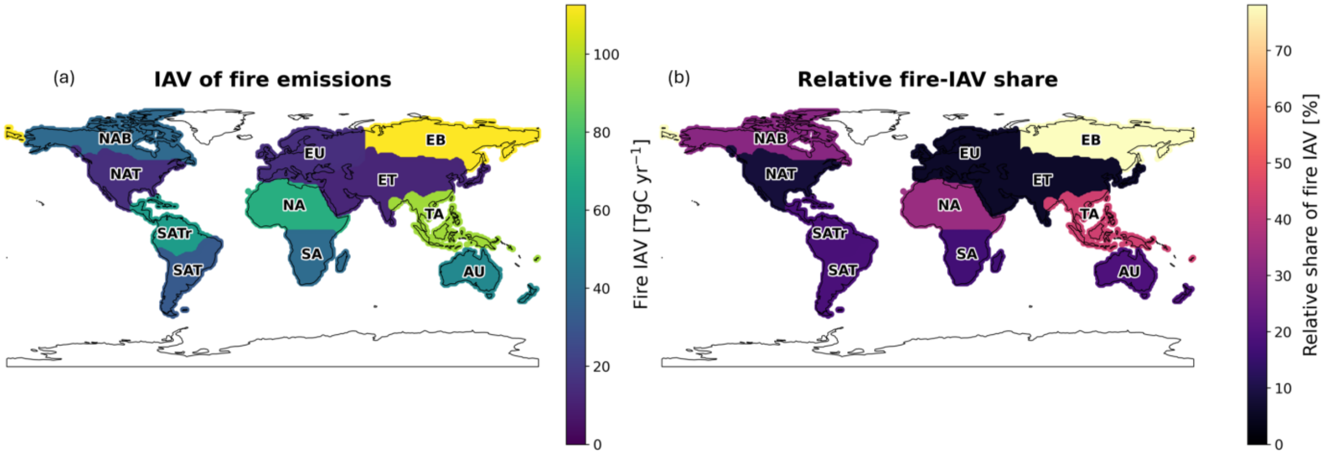

Fig. A2: Regional IAV of fire emissions over the analysis period (left) and the relative contribution of fire-emission variability to the total variability of the selected carbon-flux product (right). Fire-emission IAV is calculated as the standard deviation of annual GFEDv5 fire-emission totals for each TransCom region. The relative contribution is expressed as the ratio of fire-emission IAV to the absolute IAV of the corresponding regional carbon flux. Regions with large fire variability, particularly Eurasia Boreal, Tropical Asia, and Northern Africa, show a comparatively strong contribution of fire to total carbon-flux variability.

https://doi.org/10.5194/egusphere-2026-4054
Preprint. Discussion started: 15 July 2026

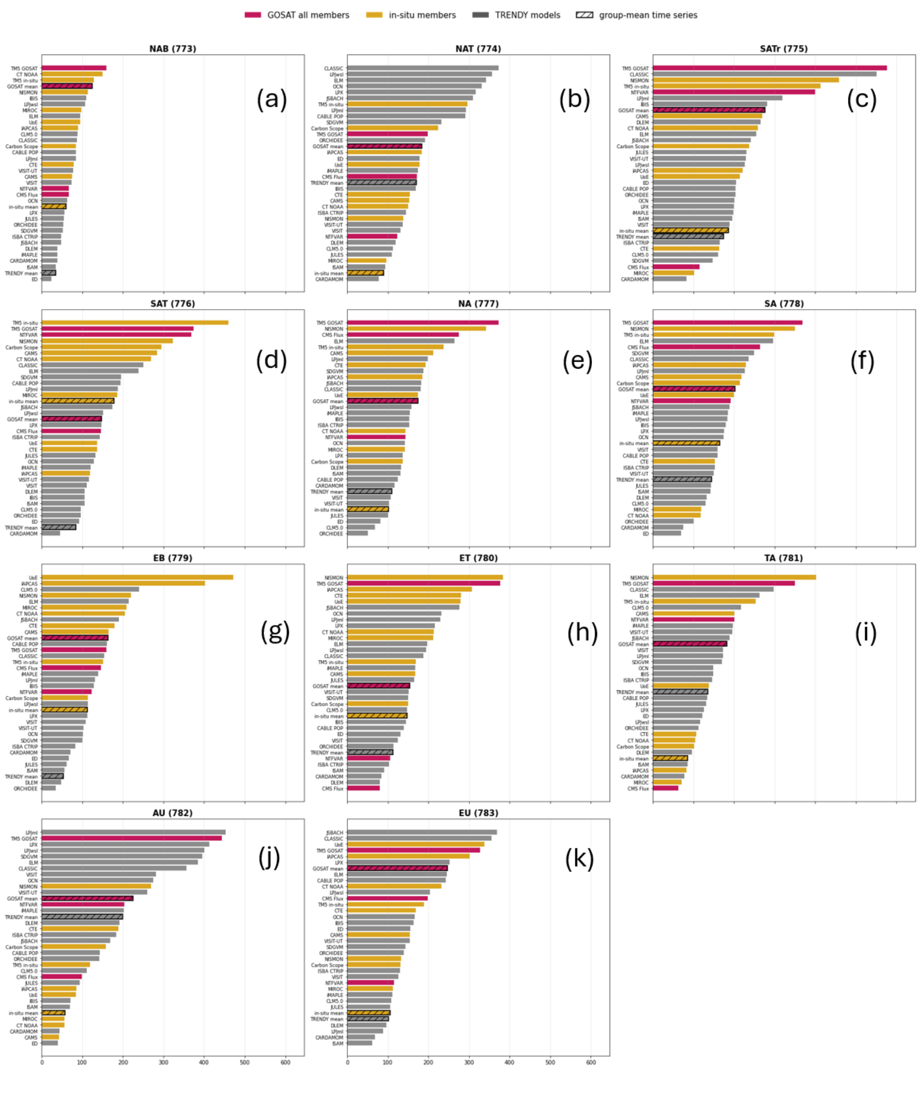

Figure A3: IAV of individual flux products per region. For each TransCom region, bars show the IAV of annual NEE for individual flux products and models over 2009–2022, sorted from low to high IAV. IAV is calculated as the standard deviation of NEE totals. Colours distinguish the three product families: GOSAT-constrained inversions, including TM5-4DVAR GOSAT, CMS-Flux, and NTFVAR; in-situ-based inversions, including TM5-4DVAR in-situ and the GCP in-situ-only ensemble members; and individual TRENDY models. Hatched bars indicate the IAV of the corresponding group-mean time series, calculated after averaging the monthly fluxes within each group, rather than as the mean of individual-member IAV values. The figure illustrates the spread of IAV estimates within each observational/model family and highlights regions where GOSAT-constrained products show stronger variability than in-situ-only inversions or TRENDY models.

https://doi.org/10.5194/egusphere-2026-4054
Preprint. Discussion started: 15 July 2026

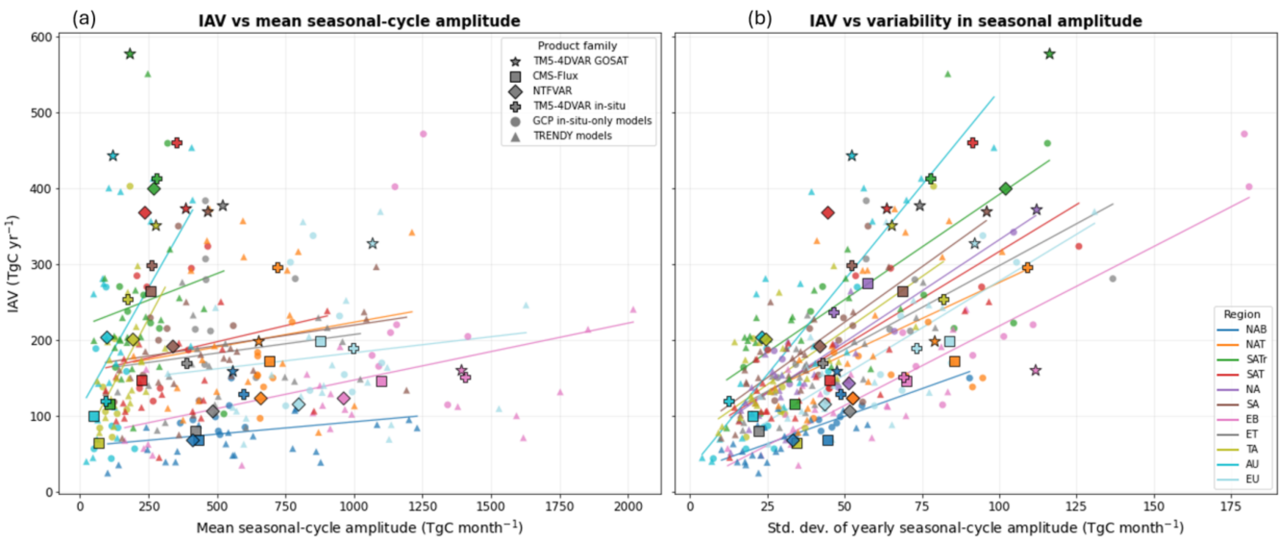

Fig. A4. Left: Relationship between mean seasonal-cycle amplitude and IAV of regional NEE. Right: Relationship between the standard deviation of yearly seasonal-cycle amplitude and IAV. Each point represents one flux product or model for one TransCom region. Colours indicate regions, and marker shapes distinguish TRENDY models, GCP in-situ-only inversions, TM5-4DVAR in-situ and GOSAT inversions, CMS-Flux, and NTFVAR. Lines show separate linear regressions for each region. The positive relationships indicate that products and models with larger seasonal exchange tend to exhibit larger IAV, with the tighter relationship in the right panel suggesting that year-to-year variability in seasonal amplitude is more closely linked to IAV than the mean seasonal-cycle amplitude alone.

https://doi.org/10.5194/egusphere-2026-4054
Preprint. Discussion started: 15 July 2026

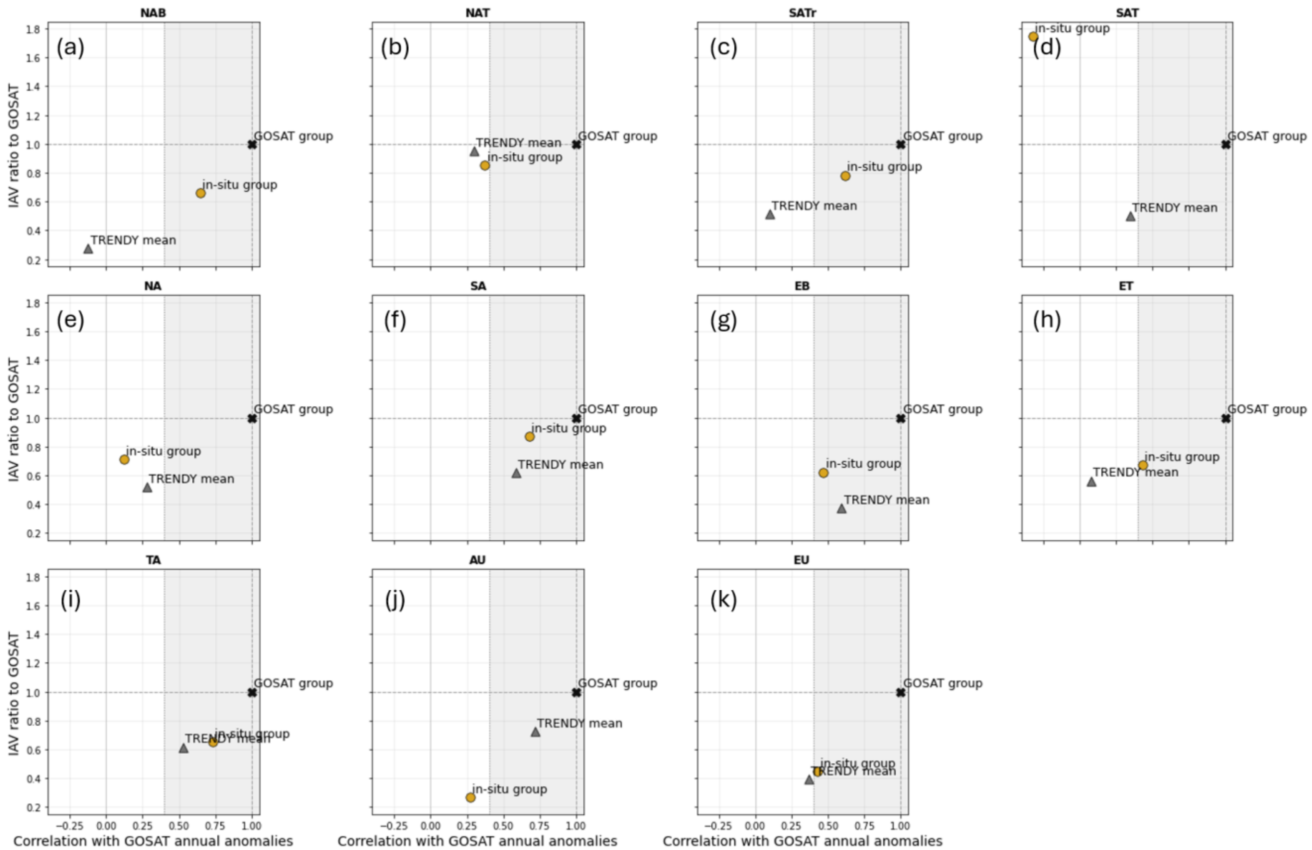

Fig. A5. Correlation of annual NEE anomalies with the GOSAT-based group mean versus relative IAV for each TransCom region. The x-axis shows the Pearson correlation with GOSAT annual anomalies, and the y-axis shows the ratio of IAV relative to GOSAT. The GOSAT-based product lies at (1,1) by definition. The in situ-only group and TRENDY ensemble mean are shown for comparison. The dashed horizontal line indicates equal IAV, and the dashed vertical line at r = 0.5 is included for visual guidance. In many regions, the in situ-only product remains moderately correlated with GOSAT but exhibits weaker IAV, whereas the TRENDY mean often shows both weaker IAV and weaker correlation, indicating that the data–model mismatch often involves both amplitude and structural differences.

https://doi.org/10.5194/egusphere-2026-4054
Preprint. Discussion started: 15 July 2026

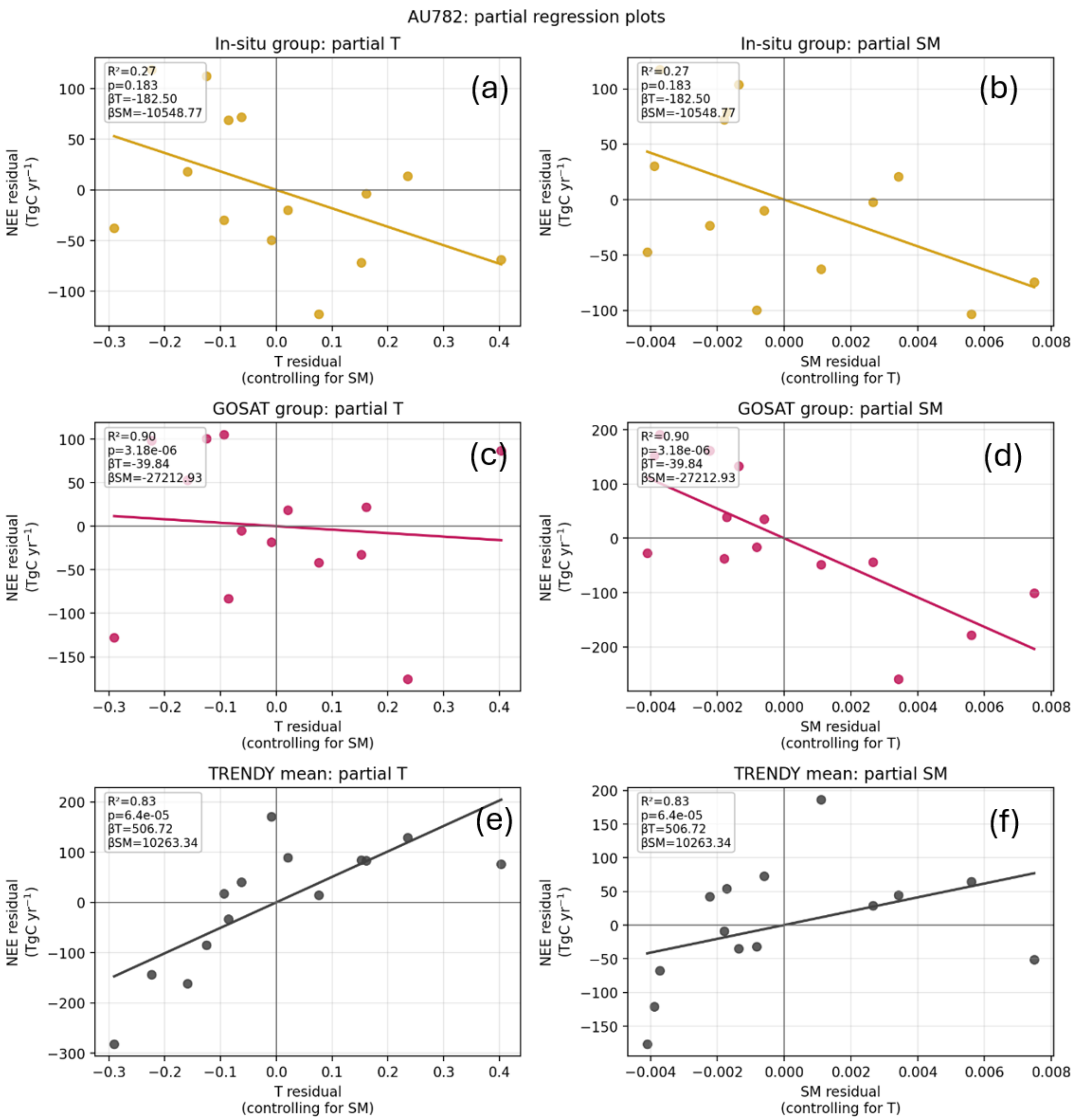

Fig. A6: Partial regression over Australia Partial regression of in-situ (upper row, yellow), GOSAT (second row, red) and TRENDY (lower row, black) for temperature anomalies (left) and soil moisture anomalies (right) over Australia (AU). The plot shows the partial regression of one climate variable, when controlling for the other. The parameters in the legend correspond to the full regression, not only the partial regression.

https://doi.org/10.5194/egusphere-2026-4054
Preprint. Discussion started: 15 July 2026

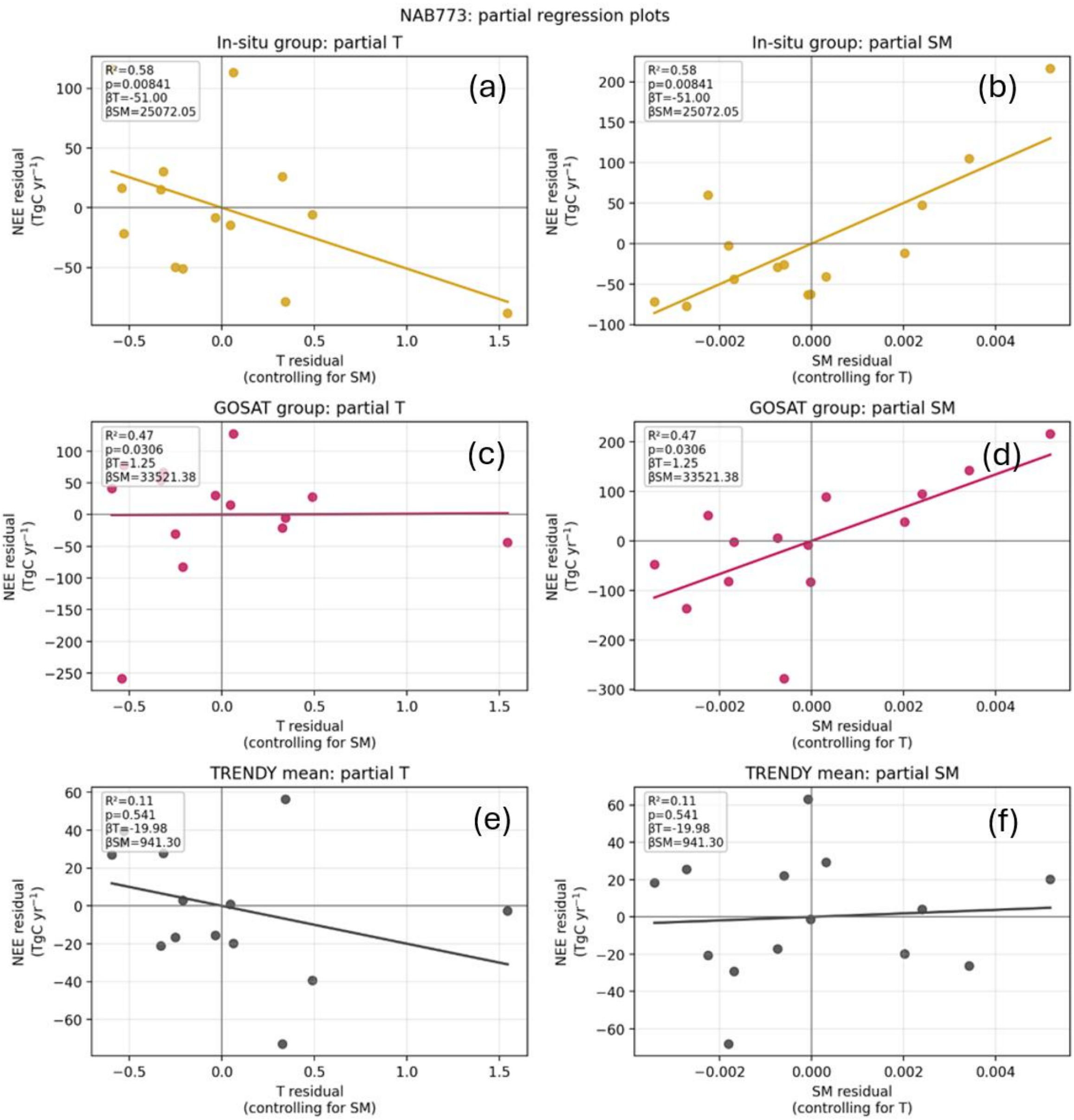

Fig. A7: Partial regression over North American Boreal. Partial regression of in-situ (upper row, yellow), GOSAT (second row, red) and TRENDY (lower row, black) for temperature anomalies (left) and soil moisture anomalies (right) over North American Boreal (NAB). The plot shows the partial regression of one climate variable, when controlling for the other. . The parameters in the legend correspond to the full regression, not only the partial regression.

https://doi.org/10.5194/egusphere-2026-4054
Preprint. Discussion started: 15 July 2026

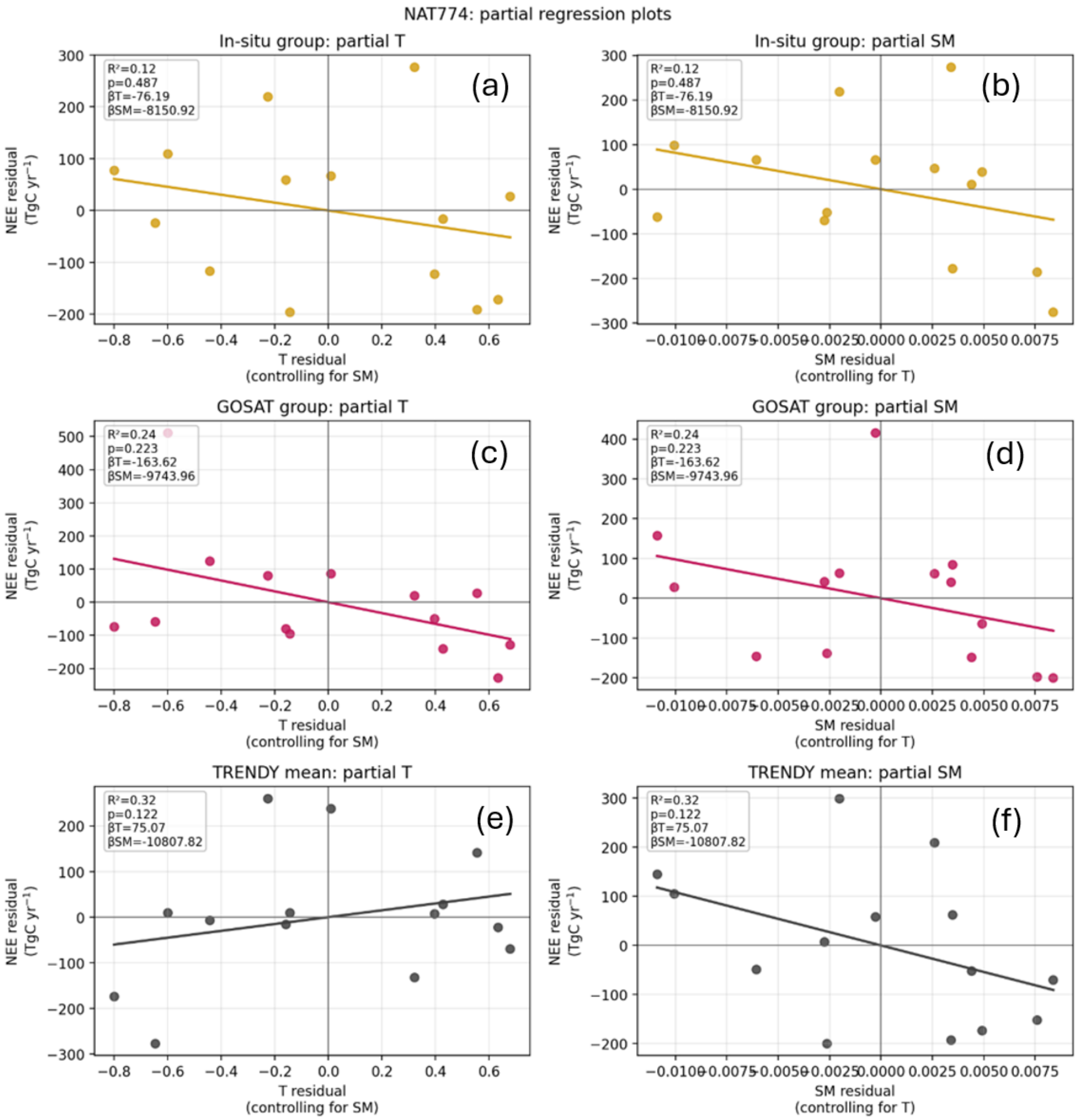

Fig. A8: Partial regression over North American Temperate. Partial regression of in-situ (upper row, yellow), GOSAT (second row, red) and TRENDY (lower row, black) for temperature anomalies (left) and soil moisture anomalies (right) over North American Temperate (NAT). The plot shows the partial regression of one climate variable, when controlling for the other. The parameters in the legend correspond to the full regression, not only the partial regression.

https://doi.org/10.5194/egusphere-2026-4054
Preprint. Discussion started: 15 July 2026

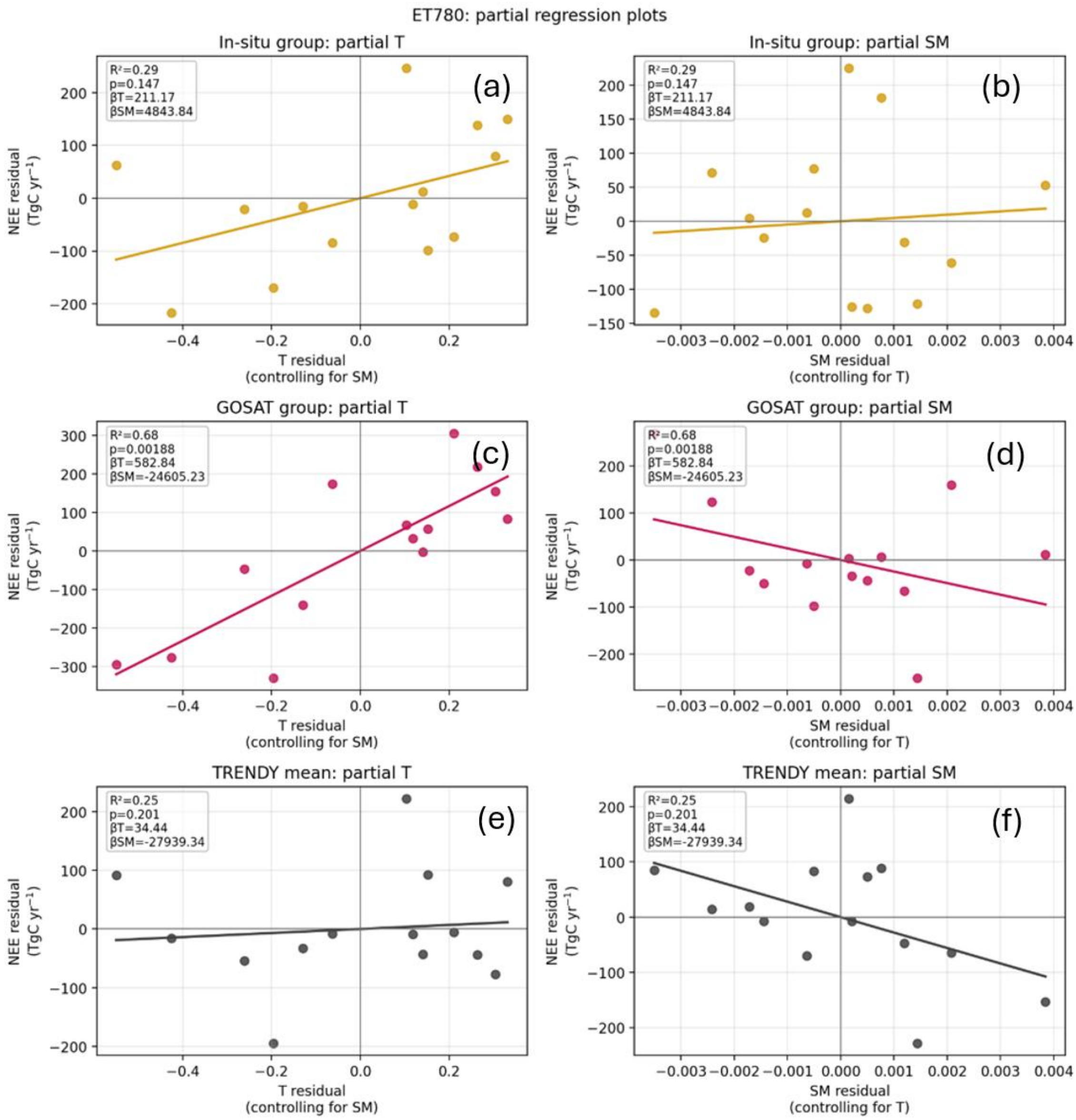

Fig. A9: Partial regression over Eurasia Temperate. Partial regression of in-situ (upper row, yellow), GOSAT (second row, red) and TRENDY (lower row, black) for temperature anomalies (left) and soil moisture anomalies (right) over Eurasia Temperate (ET). The plot shows the partial regression of one climate variable, when controlling for the other. The parameters
550 in the legend correspond to the full regression, not only the partial regression.

https://doi.org/10.5194/egusphere-2026-4054
Preprint. Discussion started: 15 July 2026

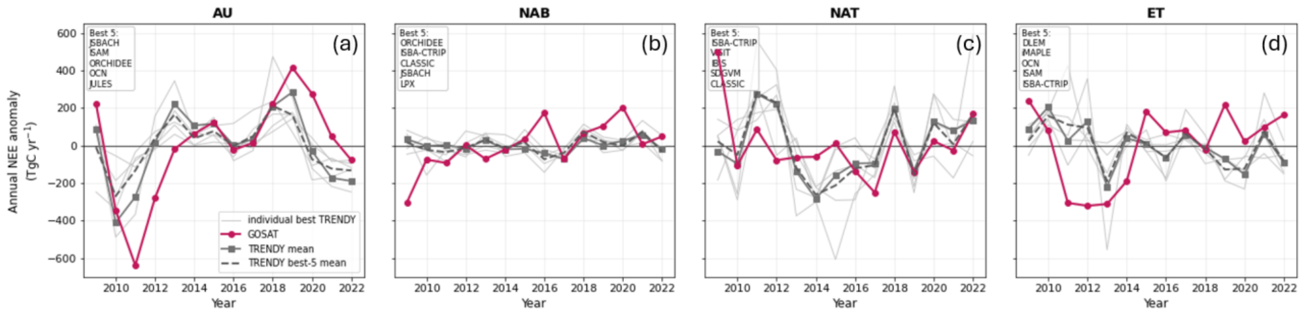

Fig. A10. Annual NEE anomalies for the GOSAT-based product (pink), the TRENDY ensemble mean (gray), the mean of the five TRENDY models with the lowest monthly RMSE relative to GOSAT (gray dashed), and the individual five selected TRENDY models (thin gray) for the four focus regions. The annual anomaly structure of the best-performing TRENDY models remains close to the TRENDY ensemble mean and still differs from the GOSAT-based estimate in the key regions. This indicates that the identified data–model mismatch is not restricted to poorly performing DGVMs, but is also present within a subset of TRENDY models selected for relatively good agreement with monthly GOSAT variability.

https://doi.org/10.5194/egusphere-2026-4054
Preprint. Discussion started: 15 July 2026

Product / system	Observation constraint	Transport model	Prior land flux	Optimization	Reference
TM5-4DVAR IS	In situ CO_2	TM5	CASA climatology	Weekly, 3° × 2°	Basu et al., 2013
CarboScope	In situ CO_2	TM3	Zero land prior	Monthly, 2° × 2.5°	Rödenbeck et al., 2003
CAMS	In situ CO_2	LMDZv6	ORCHIDEE	Weekly, gridded	Chevallier et al., 2005
CTE	In situ CO_2	TM5	SiB4	Weekly, 1° × 1° / ecoregions	van der Laan-Luijkx et al., 2017
NISMON	In situ CO_2	NICAM-TM	VISIT	Monthly mean + 3-hourly scaling	Niwa et al., 2022
CT-NOAA	In situ CO_2	TM5	Multiple priors	Weekly, ecoregions	Jacobson et al., 2023
UoE	In situ CO_2	GEOS-Chem	CASA climatology	Monthly regional fluxes	Palmer et al., 2019
IAPCAS	In situ CO_2	GEOS-Chem	CASA climatology	Monthly regional fluxes	Feng et al., 2016; Yang et al., 2021
MIROC	In situ CO_2	MIROC4-ACTM	CASA	Monthly regional fluxes	Chandra et al., 2022; Patra et al., 2018
TM5-4DVAR GOSAT+IS	GOSAT XCO_2 + in situ CO_2	TM5	CASA climatology	Weekly, 3° × 2°	Basu et al., 2013
CMS-Flux	GOSAT + OCO-2 + in situ CO_2	GEOS-Chem	CARDAMOM	Monthly, 4° × 5°	Liu et al., 2021
NTFVAR	GOSAT + in situ CO_2	NIES-TM-FLEXPART	Zeng et al. prior	Biweekly scaling	Maksyutov et al., 2021; Nayagam et al., 2025

575 **Table A1**: Overview over top-down estimates used.

https://doi.org/10.5194/egusphere-2026-4054
Preprint. Discussion started: 15 July 2026

TRENDY model	Scenario	Native resolution	Fluxes used to calculate NEE in this study	Reference
CABLE-POP	S3	0.5° × 0.5°	NBP	Haverd et al., 2018
CARDAMOM	S3	1° × 1°	NBP − fire	Smallman et al., 2021
CLASSIC	S3	2.80° × 2.81°	RA + RH + FLUC − GPP	Melton et al., 2020
CLM6.0	S3	0.9° × 1.25°	RA + RH + FLUC − GPP	Lawrence et al., 2019
DLEM	S3	0.5° × 0.5°	RA + RH − GPP	Tian et al., 2015
EDv3	S3	1° × 1°	NBP − fire	Ma et al., 2022
ELM	S3	1° × 1°	NBP − fire	Burrows et al. 2020
IBIS	S3	1° × 1°	NBP	Xia et al. 2024
IMAPLE	S3	1° × 1°	NBP	Yue et al., 2024
ISAM	S3	0.5° × 0.5°	RA + RH − GPP	Meiyappan et al., 2015
ISBA-CTRIP	S3	1° × 1°	NBP − fire	Delire et al., 2020
JSBACH	S3	1.86∘ × 1.88∘	NBP-fire	Reick et al., 2021
JULES	S3	1.25° × 1.88°	NBP − fire	Sellar et al., 2019
LPJ-GUESS	S3	1° × 1°	Not used	Smith et al., 2014
LPJmL	S3	0.5° × 0.5°	RA + RH − GPP	Schaphoff et al., 2018
LPJ-wsl	S3	0.5° × 0.5°	RA + RH − GPP	Calle and Poulter, 2021
LPX-Bern	S3	0.5° × 0.5°	NBP − fire	Lienert and Joos, 2018
ORCHIDEE	S3	0.5° × 0.5°	NBP − fire	Vuichard et al., 2019
OCN	S3	1° × 1°	NBP	Zaehle and Friend, 2010
SDGVM	S3	1° × 1°	NBP − fire	Walker et al., 2017
VISIT	S3	0.5° × 0.5°	RA + RH + FLUC − GPP	Kato et al., 2013
VISIT-UT	S3	0.5° × 0.5°	RA + RH + FLUC − GPP	Ito and Inatomi, 2012

Table A2. TRENDYv13 DGVM used in this study. All models are taken from the S3 experiment. NEE is constructed using the atmospheric sign convention, where positive fluxes denote CO_2 release from the land to the atmosphere and negative fluxes denote net land uptake. Depending on model output availability, NEE is either derived from NBP with fire removed, or

https://doi.org/10.5194/egusphere-2026-4054
Preprint. Discussion started: 15 July 2026

reconstructed from component fluxes as respiration plus land-use change minus GPP. LPJ-GUESS was excluded from the NEE analysis as monthly fluxes were not available.

Data availability

We use GOSAT and in-situ based global top-down CO_2 flux inversions from Luijkx et al., 2025), which have been further described in van der Woude et al., 2025). Additionally, we add a TM5-4DVAR top-down inversion using in-situ only and in-situ plus GOSAT XCO2 data. The XCO2 data was analysed using the RemoTeCv2.4.1 full-physics algorithm and is available here: https://zenodo.org/records/12773070. Fire emissions from GFEDv5 van der Werf et al., 2025) are available at https://www.globalfiredata.org. The TRENDY model data v13 is available from https://mdosullivan.github.io/GCB/. ERA5-Land reanalysis data have been downloaded from: https://cds.climate.copernicus.eu/datasets/reanalysis-era5-land

Author contributions

SNV designed the study, conducted the analysis and wrote the original manuscript. AB and EMM retrieved the XCO_2 estimates from GOSAT using RemoteC. SB conducted the global inversion using TM5-4DVAR. All authors commented on the manuscript.

Competing interests

We declare no competing interests.

Acknowledgements

The authors thank the in-situ data providers for making their data available through ObsPack. The authors also thank Stephen Sitch, Pierre Friedlingstein, and all modellers of version 13 of the TRENDY project "Trends and drivers of the regional-scale terrestrial sources and sinks of carbon dioxide"). This work used resources of the Deutsches Klimarechenzentrum DKRZ) granted by its Scientific Steering Committee WLA) under project ID bb1170. The authors gratefully acknowledge the data storage service SDS@hd, supported by the Ministry of Science, Research and the Arts Baden-Württemberg MWK), and the German Research Foundation DFG) through grant INST 35/1503-1 FUGG. Generative AI tools were used for minor language editing of individual sentences and for limited technical assistance with code testing, commenting, and plotting. All scientific analyses, interpretations, conclusions, and the substantive writing of the manuscript were carried out by the authors.

https://doi.org/10.5194/egusphere-2026-4054
Preprint. Discussion started: 15 July 2026

References

Ahlström, A., Raupach, M. R., Schurgers, G., Smith, B., Arneth, A., Jung, M., Reichstein, M., Canadell, J. G., Friedlingstein, P., Jain, A. K., Kato, E., Poulter, B., Sitch, S., Stocker, B. D., Viovy, N., Wang, Y. P., Wiltshire, A., Zaehle, S., and Zeng, N.: Carbon cycle. The dominant role of semi-arid ecosystems in the trend and variability of the land CO_2 sink, Science New York, N.Y.), 348, 895–899, doi:10.1126/science.aaa1668, 2015.

Bastos, A., Friedlingstein, P., Sitch, S., Chen, C., Mialon, A., Wigneron, J.-P., Arora, V. K., Briggs, P. R., Canadell, J. G., Ciais, P., Chevallier, F., Cheng, L., Delire, C., Haverd, V., Jain, A. K., Joos, F., Kato, E., Lienert, S., Lombardozzi, D., Melton, J. R., Myneni, R., Nabel, J. E. M. S., Pongratz, J., Poulter, B., Rödenbeck, C., Séférian, R., Tian, H., van Eck, C., Viovy, N., Vuichard, N., Walker, A. P., Wiltshire, A., Yang, J., Zaehle, S., Zeng, N., and Zhu, D.: Impact of the 2015/2016 El Niño on the terrestrial carbon cycle constrained by bottom-up and top-down approaches, Philosophical transactions of the Royal Society of London. Series B, Biological sciences, 373, doi:10.1098/rstb.2017.0304, 2018.

Bastos, A., O'Sullivan, M., Ciais, P., Makowski, D., Sitch, S., Friedlingstein, P., Chevallier, F., Rödenbeck, C., Pongratz, J., Luijkx, I. T., Patra, P. K., Peylin, P., Canadell, J. G., Lauerwald, R., Li, W., Smith, N. E., Peters, W., Goll, D. S., Jain, A. K., Kato, E., Lienert, S., Lombardozzi, D. L., Haverd, V., Nabel, J. E. M. S., Poulter, B., Tian, H., Walker, A. P., and Zaehle, S.: Sources of Uncertainty in Regional and Global Terrestrial CO_2 Exchange Estimates, Global Biogeochemical Cycles, 34, doi:10.1029/2019GB006393, 2020.

Basu, S., Baker, D. F., Chevallier, F., Patra, P. K., Liu, J., and Miller, J. B.: The impact of transport model differences on CO_2 surface flux estimates from OCO-2 retrievals of column average CO_2, Atmos. Chem. Phys., 18, 7189–7215, doi:10.5194/acp-18-7189-2018, 2018.

Basu, S., Guerlet, S., Butz, A., Houweling, S., Hasekamp, O., Aben, I., Krummel, P., Steele, P., Langenfelds, R., Torn, M., Biraud, S., Stephens, B., Andrews, A., and Worthy, D.: Global CO_2 fluxes estimated from GOSAT retrievals of total column CO_2, Atmos. Chem. Phys., 13, 8695–8717, doi:10.5194/acp-13-8695-2013, 2013.

Butz, A.: RemoTeC full-physics retrieval GOSAT/TANSO-FTS Level 2 bias-corrected XCO_2 2009-2023, version 2.4.1 operated at Heidelberg University, Zenodo, doi:10.5281/ZENODO.12773069, 2024.

Butz, A., Guerlet, S., Hasekamp, O., Schepers, D., Galli, A., Aben, I., Frankenberg, C., Hartmann, J.-M., Tran, H., Kuze, A., Keppel-Aleks, G., Toon, G., Wunch, D., Wennberg, P., Deutscher, N., Griffith, D., Macatangay, R., Messerschmidt, J., Notholt, J., and Warneke, T.: Toward accurate CO_2 and CH_4 observations from GOSAT, Geophysical Research Letters, 38, n/a-n/a, doi:10.1029/2011GL047888, 2011.

Byrne, B., Liu, J., Bloom, A. A., Bowman, K. W., Butterfield, Z., Joiner, J., Keenan, T. F., Keppel-Aleks, G., Parazoo, N. C., and Yin, Y.: Contrasting Regional Carbon Cycle Responses to Seasonal Climate Anomalies Across the East-West Divide of Temperate North America, Global Biogeochemical Cycles, 34, e2020GB006598, doi:10.1029/2020GB006598, 2020.

Calle, L. and Poulter, B.: Ecosystem age-class dynamics and distribution in the LPJ-wsl v2.0 global ecosystem model, Geosci. Model Dev., 14, 2575–2601, doi:10.5194/gmd-14-2575-2021, 2021.

Carle, H., Bauman, D., Evans, M. N., Coughlin, I., Binks, O., Ford, A., Bradford, M., Nicotra, A., Murphy, H., and Meir, P.: Aboveground biomass in Australian tropical forests now a net carbon source, Nature, 646, 611–618, doi:10.1038/s41586-025-09497-8, 2025.

Chandra, N., Patra, P. K., Niwa, Y., Ito, A., Iida, Y., Goto, D., Morimoto, S., Kondo, M., Takigawa, M., Hajima, T., and Watanabe, M.: Estimated regional CO_2 flux and uncertainty based on an ensemble of atmospheric CO_2 inversions, Atmos. Chem. Phys., 22, 9215–9243, doi:10.5194/acp-22-9215-2022, 2022.

Chen, Z., Liu, J., Henze, D. K., Huntzinger, D. N., Wells, K. C., Sitch, S., Friedlingstein, P., Joetzjer, E., Bastrikov, V., Goll, D. S., Haverd, V., Jain, A. K., Kato, E., Lienert, S., Lombardozzi, D. L., McGuire, P. C., Melton, J. R., Nabel, J. E. M. S., Poulter, B., Tian, H., Wiltshire, A. J., Zaehle, S., and Miller, S. M.: Linking global terrestrial CO_2 fluxes and environmental drivers: inferences from the Orbiting Carbon Observatory 2 satellite and terrestrial biospheric models, Atmos. Chem. Phys., 21, 6663–6680, doi:10.5194/acp-21-6663-2021, 2021.

Chevallier, F., Fisher, M., Peylin, P., Serrar, S., Bousquet, P., Bréon, F.-M., Chédin, A., and Ciais, P.: Inferring CO_2 sources and sinks from satellite observations: Method and application to TOVS data, J. Geophys. Res., 110, doi:10.1029/2005JD006390, 2005.

Ciais, P., Chevallier, F., Wang, Y., and Lauerwald, R.: Lateral Accounting of Transport in Terrestrial Ecosystems LATTE): A high-resolution global land-atmosphere CO_2 flux dataset from 1961 to 2022 for atmospheric inversions and carbon budgeting studies, doi:10.22541/essoar.177170483.34963512/v1, 2026.

Delire, C., Séférian, R., Decharme, B., Alkama, R., Calvet, J.-C., Carrer, D., Gibelin, A.-L., Joetzjer, E., Morel, X., Rocher, M., and Tzanos, D.: The Global Land Carbon Cycle Simulated With ISBA-CTRIP: Improvements Over the Last Decade, Journal of advances in modeling earth systems, 12, doi:10.1029/2019MS001886, 2020.

Eyre, B. D., Rosentreter, J. A., and Erler, D. V.: Significant greenhouse gas emissions from flooded drylands in Kati Thanda Lake Eyre basin in Australia, Sci Rep, 16, doi:10.1038/s41598-026-35915-6, 2026.

Feng, L., Palmer, P. I., Parker, R. J., Deutscher, N. M., Feist, D. G., Kivi, R., Morino, I., and Sussmann, R.: Estimates of European uptake of CO_2 inferred from GOSAT X CO_2 retrievals: sensitivity to measurement bias inside and outside Europe, Atmos. Chem. Phys., 16, 1289–1302, doi:10.5194/acp-16-1289-2016, 2016.

Foster, K. T., Sun, W., Shiga, Y. P., Mao, J., and Michalak, A. M.: Multiscale assessment of North American terrestrial carbon balance, Biogeosciences, 21, 869–891, doi:10.5194/bg-21-869-2024, 2024.

Friedlingstein, P., O'Sullivan, M., Jones, M. W., Andrew, R. M., Bakker, D. C. E., Hauck, J., Landschützer, P., Le Quéré, C., Li, H., Luijkx, I. T., Peters, G. P., Peters, W., Pongratz, J., Schwingshackl, C., Sitch, S., Canadell, J. G., Ciais, P., Aas, K., Alin, S. R., Anthoni, P., Barbero, L., Bates, N. R., Bellouin, N., Benoit-Cattin, A., Berghoff, C. F., Bernardello, R., Bopp, L., Brasika, I. B. M., Chamberlain, M. A., Chandra, N., Chevallier, F., Chini, L. P., Collier, N. O., Colligan, T. H., Cronin, M., Djeutchouang, L. M., Dou, X., Enright, M. P., Enyo, K., Erb, M., Evans, W., Feely, R. A., Feng, L., Ford, D. J., Foster, A., Fransner, F., Gasser, T., Gehlen, M., Gkritzalis, T., Goncalves De Souza, J., Grassi, G., Gregor, L., Gruber, N., Guenet, B., Gürses, Ö., Harrington, K., Harris, I., Heinke, J., Hurtt, G. C., Iida, Y., Ilyina, T., Ito, A., Jacobson, A. R., Jain, A. K., Jarníková, T., Jersild, A., Jiang, F., Jones, S. D., Kato, E., Keeling, R. F., Klein Goldewijk, K., Knauer, J., Kong, Y., Korsbakken, J. I., Koven, C., Kunimitsu, T., Lan, X., Liu, J., Liu, Z., Liu, Z., Lo Monaco, C., Ma, L., Marland, G., McGuire, P. C., McKinley, G. A., Melton, J. R., Monacci, N., Monier, E., Morgan, E. J., Munro, D. R., Müller, J. D., Nakaoka, S.-I., Nayagam, L. R., Niwa, Y., Nutzel, T., Olsen, A., Omar, A. M., Pan, N., Pandey, S., Pierrot, D., Qin, Z., Regnier, P., Rehder, G., Resplandy, L., Roobaert, A., Rosan, T. M., Rödenbeck, C., Schwinger, J., Skjelvan, I., Smallman, T. L., Spada, V., Sreeush, M. G., Sun, Q., Sutton, A. J., Sweeney, C., Swingedouw, D., Séférian, R., Takao, S., Tatebe, H., Tian, H., Tian, X., Tilbrook, B., Tsujino, H., Tubiello, F., van Ooijen, E., van der Werf, G. R., van de Velde, S. J., Walker, A. P., Wanninkhof, R., Yang, X., Yuan, W., Yue, X., and Zeng, J.: Global Carbon Budget 2025, Earth Syst. Sci. Data, 18, 3211–3288, doi:10.5194/essd-18-3211-2026, 2026.

Friedlingstein, P., O'Sullivan, M., Jones, M. W., Andrew, R. M., Hauck, J., Landschützer, P., Le Quéré, C., Li, H., Luijkx, I. T., Olsen, A., Peters, G. P., Peters, W., Pongratz, J., Schwingshackl, C., Sitch, S., Canadell, J. G., Ciais, P., Jackson, R. B., Alin, S. R., Arneth, A., Arora, V., Bates, N. R., Becker, M., Bellouin, N., Berghoff, C. F., Bittig, H. C., Bopp, L., Cadule, P., Campbell, K., Chamberlain, M. A., Chandra, N., Chevallier, F., Chini, L. P., Colligan, T., Decayeux, J., Djeutchouang, L. M., Dou, X., Duran Rojas, C., Enyo, K., Evans, W., Fay, A. R., Feely, R. A., Ford, D. J., Foster, A., Gasser, T., Gehlen, M., Gkritzalis, T., Grassi, G., Gregor, L., Gruber, N., Gürses, Ö., Harris, I., Hefner, M., Heinke, J., Hurtt, G. C., Iida, Y., Ilyina, T., Jacobson, A. R., Jain, A. K., Jarníková, T., Jersild, A., Jiang, F., Jin, Z., Kato, E., Keeling, R. F., Klein Goldewijk, K., Knauer, J., Korsbakken, J. I., Lan, X., Lauvset, S. K., Lefèvre, N., Liu, Z., Liu, J., Ma, L., Maksyutov, S., Marland, G., Mayot, N., McGuire, P. C., Metzl, N., Monacci, N. M., Morgan, E. J., Nakaoka, S.-I., Neill, C., Niwa, Y., Nützel, T., Olivier, L., Ono, T., Palmer, P. I., Pierrot, D., Qin, Z., Resplandy, L., Roobaert, A., Rosan, T. M., Rödenbeck, C., Schwinger, J., Smallman, T. L., Smith, S. M., Sospedra-Alfonso, R., Steinhoff, T., Sun, Q., Sutton, A. J., Séférian, R., Takao, S., Tatebe, H., Tian, H., Tilbrook, B., Torres, O., Tourigny, E., Tsujino, H., Tubiello, F., van der Werf, G., Wanninkhof, R., Wang, X., Yang, D., Yang, X., Yu, Z., Yuan, W., Yue, X., Zaehle, S., Zeng, N., and Zeng, J.: Global Carbon Budget 2024, Earth Syst. Sci. Data, 17, 965–1039, doi:10.5194/essd-17-965-2025, 2025.

Gurney, K. R., Law, R. M., Denning, A. S., Rayner, P. J., Pak, B. C., Baker, D., Bousquet, P., Bruhwiler, L., Chen, Y.-H., Ciais, P., Fung, I. Y., Heimann, M., John, J., Maki, T., Maksyutov, S., Peylin, P., Prather, M., and Taguchi, S.: Transcom 3 inversion intercomparison: Model mean results for the estimation of seasonal carbon sources and sinks, Global Biogeochemical Cycles, 18, doi:10.1029/2003GB002111, 2004.

Haverd, V., Smith, B., Nieradzik, L., Briggs, P. R., Woodgate, W., Trudinger, C. M., Canadell, J. G., and Cuntz, M.: A new version of the CABLE land surface model Subversion revision r4601) incorporating land use and land cover change, woody vegetation demography, and a novel optimisation-based approach to plant coordination of photosynthesis, Geosci. Model Dev., 11, 2995–3026, doi:10.5194/gmd-11-2995-2018, 2018.

Ito, A. and Inatomi, M.: Use of a process-based model for assessing the methane budgets of global terrestrial ecosystems and evaluation of uncertainty, Biogeosciences, 9, 759–773, doi:10.5194/bg-9-759-2012, 2012.

Jacobson, A. R., Schuldt, K. N., Tans, P., Arlyn Andrews, Miller, J. B., Oda, T., Mund, J., Weir, B., Ott, L., Aalto, T., Abshire, J. B., Aikin, K., Aoki, S., Apadula, F., Arnold, S., Baier, B., Bartyzel, J., Beyersdorf, A., Biermann, T., Biraud, S. C., Boenisch, H., Brailsford, G., Brand, W. A., Chen, G., Huilin Chen, Lukasz Chmura, Clark, S., Colomb, A., Commane, R., Conil, S., Couret, C., Cox, A., Cristofanelli, P., Cuevas, E., Curcoll, R., Daube, B., Davis, K. J., Wekker, S. de, Della Coletta, J., Delmotte, M., DiGangi, E., DiGangi, J. P., Di Sarra, A. G., Dlugokencky, E., Elkins, J. W., Emmenegger, L., Shuangxi Fang, Fischer, M. L., Forster, G., Frumau, A., Galkowski, M., Gatti, L. V., Gehrlein, T., Gerbig, C., Francois Gheusi, Gloor, E., Gomez-Trueba, V., Goto, D., Griffis, T., Hammer, S., Hanson, C., Haszpra, L., Hatakka, J., Heimann, M., Heliasz, M., Hensen, A., Hermansen, O., Hintsa, E., Holst, J., Ivakhov, V., Jaffe, D. A., Jordan, A., Joubert, W., Karion, A., Kawa, S. R., Kazan, V., Keeling, R. F., Keronen, P., Kneuer, T., Kolari, P., Kateřina Komínková, Kort, E., Kozlova, E., Krummel, P., Kubistin, D., Labuschagne, C., Lam, D. H., Lan, X., Langenfelds, R. L., Laurent, O., Laurila, T., Lauvaux, T., Lavric, J., Law, B. E., Lee, J., Lee, O. S., Lehner, I., Lehtinen, K., Leppert, R., Leskinen, A., Leuenberger, M., Levin, I., Levula, J., Lin, J., Lindauer, M., Loh, Z., Lopez, M., Luijkx, I. T., Lunder, C. R., Machida, T., Mammarella, I., Manca, G., Manning, A., Manning, A., Marek, M. V., Martin, M. Y., Matsueda, H., McKain, K., Meijer, H., Meinhardt, F., Merchant, L., N. Mihalopoulos, Miles, N. L., Miller, C. E., Mitchell, L., Mölder, M., Montzka, S., Moore, F., Moossen, H., Morgan, E., Josep-Anton Morgui, Morimoto, S., Müller-Williams, J., J. William Munger, Munro, D., Myhre, C. L., Shin-Ichiro Nakaoka, Jaroslaw Necki, Newman, S., Nichol, S., Niwa, Y., Obersteiner, F., O'Doherty, S., Paplawsky, B., Peischl, J., Peltola, O., Piacentino, S., Jean-Marc Pichon, Pickers, P., Piper, S., Pitt, J., Plass-Dülmer, C., Platt, S. M., Prinzivalli, S., Ramonet, M., Ramos, R., Reyes-Sanchez, E., Richardson, S. J., Riris, H., Rivas, P. P., Ryerson, T., Saito, K., Sargent, M., Sasakawa, M., Scheeren, B., Schuck, T., Schumacher, M., Seifert, T., Sha, M. K., Shepson, P., Shook, M., Sloop, C. D., Smith, P., Stanley, K., Steinbacher, M., Stephens, B., Sweeney, C., Thoning, K., Timas, H., Torn, M., Tørseth, K., Trisolino, P., Turnbull, J., van den Bulk, P., van Dinther, D., Vermeulen, A., Viner, B., Vitkova, G., Walker, S., Watson, A., Wofsy, S. C., Worsey, J., Worthy, D., Dickon Young, Zaehle, S., Zahn, A., and Miroslaw Zimnoch: CarbonTracker CT2022, doi:10.25925/Z1GJ-3254, 2023.

Jiang, D., Yu, Z., Wang, J., Hao, M., Zhang, X., Yan, X., Liu, J., Li, Z., and Liu, Z.: Interannual variations in terrestrial carbon uptake are dominated by temperature and the vapor pressure deficit rather than water availability, npj Clim Atmos Sci, doi:10.1038/s41612-026-01440-6, 2026.

Jung, M., Schwalm, C., Migliavacca, M., Walther, S., Camps-Valls, G., Koirala, S., Anthoni, P., Besnard, S., Bodesheim, P., Carvalhais, N., Chevallier, F., Gans, F., Goll, D. S., Haverd, V., Köhler, P., Ichii, K., Jain, A. K., Liu, J., Lombardozzi, D., Nabel, J. E. M. S., Nelson, J. A., O'Sullivan, M., Pallandt, M., Papale, D., Peters, W., Pongratz, J., Rödenbeck, C., Sitch, S., Tramontana, G., Walker, A., Weber, U., and Reichstein, M.: Scaling carbon fluxes from eddy covariance sites to globe: synthesis and evaluation of the FLUXCOM approach, Biogeosciences, 17, 1343–1365, doi:10.5194/bg-17-1343-2020, 2020.

Kato, E., Kinoshita, T., Ito, A., Kawamiya, M., and Yamagata, Y.: Evaluation of spatially explicit emission scenario of land-use change and biomass burning using a process-based biogeochemical model, Journal of Land Use Science, 8, 104–122, doi:10.1080/1747423X.2011.628705, 2013.

Lawrence, D. M., Fisher, R. A., Koven, C. D., Oleson, K. W., Swenson, S. C., Bonan, G., Collier, N., Ghimire, B., van Kampenhout, L., Kennedy, D., Kluzek, E., Lawrence, P. J., Li, F., Li, H., Lombardozzi, D., Riley, W. J., Sacks, W. J., Shi, M., Vertenstein, M., Wieder, W. R., Xu, C., Ali, A. A., Badger, A. M., Bisht, G., van den Broeke, M., Brunke, M. A., Burns, S. P., Buzan, J., Clark, M., Craig, A., Dahlin, K., Drewniak, B., Fisher, J. B., Flanner, M., Fox, A. M., Gentine, P., Hoffman, F., Keppel-Aleks, G., Knox, R., Kumar, S., Lenaerts, J., Leung, L. R., Lipscomb, W. H., Lu, Y., Pandey, A., Pelletier, J. D., Perket, J., Randerson, J. T., Ricciuto, D. M., Sanderson, B. M., Slater, A., Subin, Z. M., Tang, J., Thomas, R. Q., Val Martin, M., and Zeng, X.: The Community Land Model Version 5: Description of New Features, Benchmarking, and Impact of Forcing Uncertainty, Journal of advances in modeling earth systems, 11, 4245–4287, doi:10.1029/2018MS001583, 2019.

Lienert, S. and Joos, F.: A Bayesian ensemble data assimilation to constrain model parameters and land-use carbon emissions, Biogeosciences, 15, 2909–2930, doi:10.5194/bg-15-2909-2018, 2018.

Lin, S., Hu, Z., Wang, Y., Chen, X., He, B., Song, Z., Sun, S., Wu, C., Zheng, Y., Xia, X., Liu, L., Tang, J., Sun, Q., Joos, F., and Yuan, W.: Underestimated Interannual Variability of Terrestrial Vegetation Production by Terrestrial Ecosystem Models, Global Biogeochemical Cycles, 37, doi:10.1029/2023GB007696, 2023.

Liu, J., Baskaran, L., Bowman, K., Schimel, D., Bloom, A. A., Parazoo, N. C., Oda, T., Carroll, D., Menemenlis, D., Joiner, J., Commane, R., Daube, B., Gatti, L. V., McKain, K., Miller, J., Stephens, B. B., Sweeney, C., and Wofsy, S.: Carbon Monitoring System Flux Net Biosphere Exchange 2020 CMS-Flux NBE 2020), Earth Syst. Sci. Data, 13, 299–330, doi:10.5194/essd-13-299-2021, 2021.

Luijkx, I., Peters, W., van der Woude, A., Rödenbeck, C., Chevallier, F., Martinez, A., Niwa, Y., Maity, S., Jacobson, A. R., Liu, J., Bowman, K., Yun, J., Bloom, A., Jin, Z., Tian, X., Piao, S., Wang, Y., Zhang, H., Zhao, M., Wang, T., Ding, J., Liu, Z., Zeng, N., Jiang, F., Ju, W., Feng, L., Palmer, P., Chandra, N., Patra, P., Maksyutov, S., Nayagam, L., Janardanan, R., Kong, Y., and Zheng, B.: Global CO_2 gridded flux fields from 14 atmospheric inversions in GCB2025, ICOS ERIC -- Carbon Portal, doi:10.18160/VZ3B-GHYQ, 2025.

Ma, L., Hurtt, G., Ott, L., Sahajpal, R., Fisk, J., Lamb, R., Tang, H., Flanagan, S., Chini, L., Chatterjee, A., and Sullivan, J.: Global evaluation of the Ecosystem Demography model ED v3.0), Geosci. Model Dev., 15, 1971–1994, doi:10.5194/gmd-15-1971-2022, 2022.

MacBean, N., Scott, R. L., Biederman, J. A., Peylin, P., Kolb, T., Litvak, M. E., Krishnan, P., Meyers, T. P., Arora, V. K., Bastrikov, V., Goll, D., Lombardozzi, D. L., Nabel, J. E. M. S., Pongratz, J., Sitch, S., Walker, A. P., Zaehle, S., and

https://doi.org/10.5194/egusphere-2026-4054
Preprint. Discussion started: 15 July 2026

Moore, D. J. P.: Dynamic global vegetation models underestimate net CO_2 flux mean and inter-annual variability in dryland ecosystems, Environ. Res. Lett., 16, 94023, doi:10.1088/1748-9326/ac1a38, 2021.

Maksyutov, S., Oda, T., Saito, M., Janardanan, R., Belikov, D., Kaiser, J. W., Zhuravlev, R., Ganshin, A., Valsala, V. K., Andrews, A., Chmura, L., Dlugokencky, E., Haszpra, L., Langenfelds, R. L., Machida, T., Nakazawa, T., Ramonet, M., Sweeney, C., and Worthy, D.: Technical note: A high-resolution inverse modelling technique for estimating surface CO_2 fluxes based on the NIES-TM–FLEXPART coupled transport model and its adjoint, Atmos. Chem. Phys., 21, 1245–1266, doi:10.5194/acp-21-1245-2021, 2021.

Meiyappan, P., Jain, A. K., and House, J. I.: Increased influence of nitrogen limitation on CO_2 emissions from future land use and land use change, Global Biogeochemical Cycles, 29, 1524–1548, doi:10.1002/2015GB005086, 2015.

Melton, J. R., Arora, V. K., Wisernig-Cojoc, E., Seiler, C., Fortier, M., Chan, E., and Teckentrup, L.: CLASSIC v1.0: the open-source community successor to the Canadian Land Surface Scheme CLASS) and the Canadian Terrestrial Ecosystem Model CTEM) – Part 1: Model framework and site-level performance, Geosci. Model Dev., 13, 2825–2850, doi:10.5194/gmd-13-2825-2020, 2020.

Metz, E.-M., Vardag, S. N., Basu, S., Jung, M., Ahrens, B., El-Madany, T., Sitch, S., Arora, V. K., Briggs, P. R., Friedlingstein, P., Goll, D. S., Jain, A. K., Kato, E., Lombardozzi, D., Nabel, J. E. M. S., Poulter, B., Séférian, R., Tian, H., Wiltshire, A., Yuan, W., Yue, X., Zaehle, S., Deutscher, N. M., Griffith, D. W. T., and Butz, A.: Soil respiration-driven CO_2 pulses dominate Australia's flux variability, Science New York, N.Y.), 379, 1332–1335, doi:10.1126/science.add7833, 2023.

Metz, E.-M., Vardag, S. N., Basu, S., Jung, M., and Butz, A.: Seasonal and inter-annual variability of carbon fluxes in southern Africa seen by GOSAT, 2024.

Metz, E.-M., Vardag, S. N., Basu, S., Jung, M., and Butz, A.: Seasonal and interannual variability in CO_2 fluxes in southern Africa seen by GOSAT, Biogeosciences, 22, 555–584, doi:10.5194/bg-22-555-2025, 2025.

Muñoz-Sabater, J., Dutra, E., Agustí-Panareda, A., Albergel, C., Arduini, G., Balsamo, G., Boussetta, S., Choulga, M., Harrigan, S., Hersbach, H., Martens, B., Miralles, D. G., Piles, M., Rodríguez-Fernández, N. J., Zsoter, E., Buontempo, C., and Thépaut, J.-N.: ERA5-Land: a state-of-the-art global reanalysis dataset for land applications, Earth Syst. Sci. Data, 13, 4349–4383, doi:10.5194/essd-13-4349-2021, 2021.

Nayagam, L., Maksyutov, S., Janardanan, R., Oda, T., Tiwari, Y. K., Sreenivas, G., Datye, A., Jain, C. D., Ratnam, M. V., Sinha, V., Hakkim, H., Terao, Y., Naja, M., Ahmed, M. K., Mukai, H., Zeng, J., Kaiser, J. W., Someya, Y., Yoshida, Y., and Matsunaga, T.: Indian Land Carbon Sink Estimated from Surface and GOSAT Observations, Remote Sensing, 17, 450, doi:10.3390/rs17030450, 2025.

Niwa, Y., Ishijima, K., Ito, A., and Iida, Y.: Toward a long-term atmospheric CO_2 inversion for elucidating natural carbon fluxes: technical notes of NISMON-CO_2 v2021.1, Prog Earth Planet Sci, 9, doi:10.1186/s40645-022-00502-6, 2022.

O'Sullivan, M., Sitch, S., Friedlingstein, P., Luijkx, I. T., Peters, W., Rosan, T. M., Arneth, A., Arora, V. K., Chandra, N., Chevallier, F., Ciais, P., Falk, S., Feng, L., Gasser, T., Houghton, R. A., Jain, A. K., Kato, E., Kennedy, D., Knauer, J., McGrath, M. J., Niwa, Y., Palmer, P. I., Patra, P. K., Pongratz, J., Poulter, B., Rödenbeck, C., Schwingshackl, C., Sun, Q., Tian, H., Walker, A. P., Yang, D., Yuan, W., Yue, X., and Zaehle, S.: The key role of forest disturbance in reconciling estimates of the northern carbon sink, Commun Earth Environ, 5, doi:10.1038/s43247-024-01827-4, 2024.

O'Dell, C. W., Connor, B., Bösch, H., O'Brien, D., Frankenberg, C., Castano, R., Christi, M., Eldering, D., Fisher, B., Gunson, M., McDuffie, J., Miller, C. E., Natraj, V., Oyafuso, F., Polonsky, I., Smyth, M., Taylor, T., Toon, G. C., Wennberg, P. O., and Wunch, D.: The ACOS CO_2 retrieval algorithm – Part 1: Description and validation against synthetic observations, Atmos. Meas. Tech., 5, 99–121, doi:10.5194/amt-5-99-2012, 2012.

Padrón, R. S., Gudmundsson, L., Liu, L., Humphrey, V., and Seneviratne, S. I.: Drivers of intermodel uncertainty in land carbon sink projections, Biogeosciences, 19, 5435–5448, doi:10.5194/bg-19-5435-2022, 2022.

Palmer, P. I., Feng, L., Baker, D., Chevallier, F., Bösch, H., and Somkuti, P.: Net carbon emissions from African biosphere dominate pan-tropical atmospheric CO_2 signal, Nat Commun, 10, doi:10.1038/s41467-019-11097-w, 2019.

Patra, P. K., Takigawa, M., Watanabe, S., Chandra, N., Ishijima, K., and Yamashita, Y.: Improved Chemical Tracer Simulation by MIROC4.0-based Atmospheric Chemistry-Transport Model MIROC4-ACTM), SOLA, 14, 91–96, doi:10.2151/SOLA.2018-016, 2018.

Piao, S., Wang, X., Wang, K., Li, X., Bastos, A., Canadell, J. G., Ciais, P., Friedlingstein, P., and Sitch, S.: Interannual variation of terrestrial carbon cycle: Issues and perspectives, Global Change Biology, 26, 300–318, doi:10.1111/gcb.14884, 2020.

Poulter, B., Ciais, P., Hodson, E., Lischke, H., Maignan, F., Plummer, S., and Zimmermann, N. E.: Plant functional type mapping for earth system models, Geosci. Model Dev., 4, 993–1010, doi:10.5194/gmd-4-993-2011, 2011.

Poulter, B., Frank, D., Ciais, P., Myneni, R. B., Andela, N., Bi, J., Broquet, G., Canadell, J. G., Chevallier, F., Liu, Y. Y., Running, S. W., Sitch, S., and van der Werf, G. R.: Contribution of semi-arid ecosystems to interannual variability of the global carbon cycle, Nature, 509, 600–603, doi:10.1038/nature13376, 2014.

Reick, C. H., Gayler, V., Goll, D., Hagemann, S., Heidkamp, M., Nabel, J. E. M. S., Raddatz, T., Roeckner, E., Schnur, R., and Wilkenskjeld, S.: JSBACH 3 - The land component of the MPI Earth System Model: documentation of version 3.2, 2021.

Rödenbeck, C., Houweling, S., Gloor, M., and Heimann, M.: CO_2 flux history 1982–2001 inferred from atmospheric data using a global inversion of atmospheric transport, Atmos. Chem. Phys., 3, 1919–1964, doi:10.5194/acp-3-1919-2003, 2003.

Schaphoff, S., Bloh, W. von, Rammig, A., Thonicke, K., Biemans, H., Forkel, M., Gerten, D., Heinke, J., Jägermeyr, J., Knauer, J., Langerwisch, F., Lucht, W., Müller, C., Rolinski, S., and Waha, K.: LPJmL4 – a dynamic global vegetation model with managed land – Part 1: Model description, Geosci. Model Dev., 11, 1343–1375, doi:10.5194/gmd-11-1343-2018, 2018.

Sellar, A. A., Jones, C. G., Mulcahy, J. P., Tang, Y., Yool, A., Wiltshire, A., O'Connor, F. M., Stringer, M., Hill, R., Palmieri, J., Woodward, S., Mora, L. de, Kuhlbrodt, T., Rumbold, S. T., Kelley, D. I., Ellis, R., Johnson, C. E., Walton, J., Abraham, N. L., Andrews, M. B., Andrews, T., Archibald, A. T., Berthou, S., Burke, E., Blockley, E., Carslaw, K., Dalvi, M., Edwards, J., Folberth, G. A., Gedney, N., Griffiths, P. T., Harper, A. B., Hendry, M. A., Hewitt, A. J., Johnson, B., Jones, A., Jones, C. D., Keeble, J., Liddicoat, S., Morgenstern, O., Parker, R. J., Predoi, V., Robertson, E., Siahaan, A., Smith, R. S., Swaminathan, R., Woodhouse, M. T., Zeng, G., and Zerroukat, M.: UKESM1: Description and Evaluation of the U.K. Earth System Model, Journal of advances in modeling earth systems, 11, 4513–4558, doi:10.1029/2019MS001739, 2019.

Sellers, P. J., Schimel, D. S., Moore, B., Liu, J., and Eldering, A.: Observing carbon cycle–climate feedbacks from space, Proc. Natl. Acad. Sci. U.S.A., 115, 7860–7868, doi:10.1073/pnas.1716613115, 2018.

Sitch, S., Friedlingstein, P., Gruber, N., Jones, S. D., Murray-Tortarolo, G., Ahlström, A., Doney, S. C., Graven, H., Heinze, C., Huntingford, C., Levis, S., Levy, P. E., Lomas, M., Poulter, B., Viovy, N., Zaehle, S., Zeng, N., Arneth, A., Bonan, G., Bopp, L., Canadell, J. G., Chevallier, F., Ciais, P., Ellis, R., Gloor, M., Peylin, P., Piao, S. L., Le Quéré, C., Smith, B., Zhu, Z., and Myneni, R.: Recent trends and drivers of regional sources and sinks of carbon dioxide, Biogeosciences, 12, 653–679, doi:10.5194/bg-12-653-2015, 2015.

Sitch, S., O'Sullivan, M., Robertson, E., Friedlingstein, P., Albergel, C., Anthoni, P., Arneth, A., Arora, V. K., Bastos, A., Bastrikov, V., Bellouin, N., Canadell, J. G., Chini, L., Ciais, P., Falk, S., Harris, I., Hurtt, G., Ito, A., Jain, A. K., Jones, M. W., Joos, F., Kato, E., Kennedy, D., Klein Goldewijk, K., Kluzek, E., Knauer, J., Lawrence, P. J., Lombardozzi, D., Melton, J. R., Nabel, J. E. M. S., Pan, N., Peylin, P., Pongratz, J., Poulter, B., Rosan, T. M., Sun, Q., Tian, H., Walker, A. P., Weber, U., Yuan, W., Yue, X., and Zaehle, S.: Trends and Drivers of Terrestrial Sources and Sinks of Carbon Dioxide: An Overview of the TRENDY Project, Global Biogeochemical Cycles, 38, doi:10.1029/2024GB008102, 2024.

Smallman, T. L., Milodowski, D. T., Neto, E. S., Koren, G., Ometto, J., and Williams, M.: Parameter uncertainty dominates C-cycle forecast errors over most of Brazil for the 21st century, Earth Syst. Dynam., 12, 1191–1237, doi:10.5194/esd-12-1191-2021, 2021.

Smith, B., Wårlind, D., Arneth, A., Hickler, T., Leadley, P., Siltberg, J., and Zaehle, S.: Implications of incorporating N cycling and N limitations on primary production in an individual-based dynamic vegetation model, Biogeosciences, 11, 2027–2054, doi:10.5194/bg-11-2027-2014, 2014.

Teckentrup, L., Kauwe, M. G. de, Pitman, A. J., Goll, D. S., Haverd, V., Jain, A. K., Joetzjer, E., Kato, E., Lienert, S., Lombardozzi, D., McGuire, P. C., Melton, J. R., Nabel, J. E. M. S., Pongratz, J., Sitch, S., Walker, A. P., and Zaehle, S.: Assessing the representation of the Australian carbon cycle in global vegetation models, Biogeosciences, 18, 5639–5668, doi:10.5194/bg-18-5639-2021, 2021.

Tian, H., Chen, G., Lu, C., Xu, X., Hayes, D. J., Ren, W., Pan, S., Huntzinger, D. N., and Wofsy, S. C.: North American terrestrial CO_2 uptake largely offset by CH_4 and N_2O emissions: toward a full accounting of the greenhouse gas budget, Climatic Change, 129, 413–426, doi:10.1007/s10584-014-1072-9, 2015.

van der Laan-Luijkx, I. T., van der Velde, I. R., van der Veen, E., Tsuruta, A., Stanislawska, K., Babenhauserheide, A., Zhang, H. F., Liu, Y., He, W., Chen, H., Masarie, K. A., Krol, M. C., and Peters, W.: The CarbonTracker Data Assimilation Shell CTDAS) v1.0: implementation and global carbon balance 2001–2015, Geosci. Model Dev., 10, 2785–2800, doi:10.5194/gmd-10-2785-2017, 2017.

van der Werf, G. R., Randerson, J. T., Giglio, L., van Leeuwen, T. T., Chen, Y., Rogers, B. M., Mu, M., van Marle, M. J. E., Morton, D. C., Collatz, G. J., Yokelson, R. J., and Kasibhatla, P. S.: Global fire emissions estimates during 1997–2016, Earth Syst. Sci. Data, 9, 697–720, doi:10.5194/essd-9-697-2017, 2017.

van der Werf, G. R., Randerson, J. T., van Wees, D., Chen, Y., Giglio, L., Hall, J., Vernooij, R., Mu, M., Binte Shahid, S., Barsanti, K. C., Yokelson, R., and Morton, D. C.: Landscape fire emissions from the 5th version of the Global Fire Emissions Database GFED5), Scientific data, 12, 1870, doi:10.1038/s41597-025-06127-w, 2025.

van der Woude, A., Luijkx, I. T., Kok, R. de, Peters, W., Chevallier, F., Rödenbeck, C., Ciais, P., Chandra, N., Wang, K., ACHARI, R. J., van Asperen, H., Bastos, A., van Berg, A.-W. den, Bloom, A. A., Botía, S., Bowman, K. W., Canadell, J. G., Souza, R. A. F. de, Dias-Junior, C. Q., Feng, L., Friedlingstein, P., Gatti, L. V., Gloor, E., Ishijima, K., Jiang, F., Jin, Z., Ju, W., Lan, X., Liu, J., Liu, Z., Machida, T., Maksyutov, S., Manning, A. C., Martinez, A., Martins, G., McKain, K., Miller, J. B., Nayagam, L., Niwa, Y., Stephens, B. B., Sweeney, C., Palmer, P., Patra, P. K., Pickers, P. A., Poulter, B., Wofsy, S. C. C., Wu, Z., Yang, D., Yun, J., and Zeng, N.: A top-down view of global and regional carbon budgets from an ensemble of atmospheric inversions, 2025.

Vardag, S. N., Metz, E.-M., Artelt, L., Basu, S., and Butz, A.: CO_2 Release During Soil Rewetting Shapes the Seasonal Carbon Dynamics in South American Temperate Region, Geophysical Research Letters, 52, doi:10.1029/2024GL111725, 2025.

Villalobos, Y., Rayner, P., Thomas, S., and Silver, J.: The potential of Orbiting Carbon Observatory-2 data to reduce the uncertainties in CO_2 surface fluxes over Australia using a variational assimilation scheme, Atmos. Chem. Phys., 20, 8473–8500, doi:10.5194/acp-20-8473-2020, 2020.

Vuichard, N., Messina, P., Luyssaert, S., Guenet, B., Zaehle, S., Ghattas, J., Bastrikov, V., and Peylin, P.: Accounting for carbon and nitrogen interactions in the global terrestrial ecosystem model ORCHIDEE trunk version, rev 4999): multi-scale evaluation of gross primary production, Geosci. Model Dev., 12, 4751–4779, doi:10.5194/gmd-12-4751-2019, 2019.

Walker, A. P., Quaife, T., van Bodegom, P. M., Kauwe, M. G. de, Keenan, T. F., Joiner, J., Lomas, M. R., MacBean, N., Xu, C., Yang, X., and Woodward, F. I.: The impact of alternative trait-scaling hypotheses for the maximum photosynthetic carboxylation rate Vcmax) on global gross primary production, The New phytologist, 215, 1370–1386, doi:10.1111/nph.14623, 2017.

Wang, K., Bastos, A., Ciais, P., Wang, X., Rödenbeck, C., Gentine, P., Chevallier, F., Humphrey, V. W., Huntingford, C., O'Sullivan, M., Seneviratne, S. I., Sitch, S., and Piao, S.: Regional and seasonal partitioning of water and temperature controls on global land carbon uptake variability, Nat Commun, 13, 3469, doi:10.1038/s41467-022-31175-w, 2022.

Wen, J., Sun, W., Foster, K. T., Bond-Lamberty, B., Miller, C. E., Feng, L., and Michalak, A. M.: Atmospheric CO_2 observations reveal seasonality bias in Arctic–boreal carbon flux estimates, Environ. Res. Lett., 21, 94029, doi:10.1088/1748-9326/ae6128, 2026.

Yang, D., Liu, Y., Feng, L., Wang, J., Yao, L., Cai, Z., Zhu, S., Lu, N., and Lyu, D.: The First Global Carbon Dioxide Flux Map Derived from TanSat Measurements, Adv. Atmos. Sci., 38, 1433–1443, doi:10.1007/s00376-021-1179-7, 2021.

Yoshida, Y., Kikuchi, N., Morino, I., Uchino, O., Oshchepkov, S., Bril, A., Saeki, T., Schutgens, N., Toon, G. C., Wunch, D., Roehl, C. M., Wennberg, P. O., Griffith, D. W. T., Deutscher, N. M., Warneke, T., Notholt, J., Robinson, J., Sherlock, V., Connor, B., Rettinger, M., Sussmann, R., Ahonen, P., Heikkinen, P., Kyrö, E., Mendonca, J., Strong, K., Hase, F., Dohe, S., and Yokota, T.: Improvement of the retrieval algorithm for GOSAT SWIR XCO_2 and XCH_4 and their validation using TCCON data, Atmos. Meas. Tech., 6, 1533–1547, doi:10.5194/amt-6-1533-2013, 2013.

Yue, X., Zhou, H., Tian, C., Ma, Y., Hu, Y., Gong, C., Zheng, H., and Liao, H.: Development and evaluation of the interactive Model for Air Pollution and Land Ecosystems iMAPLE) version 1.0, Geosci. Model Dev., 17, 4621–4642, doi:10.5194/gmd-17-4621-2024, 2024.

Yun, J., Liu, J., Baker, D. F., Basu, S., Chevallier, F., Jiang, F., Johnson, M. S., Li, X., Liu, Z., Miller, S. M., Philip, S., Vardag, S. N., Xiao, J., and Zeng, N.: Interannual Variability in African Regional Ecosystem Carbon Fluxes and Their Drivers Revealed by Satellite Observations, Global Biogeochemical Cycles, 39, doi:10.1029/2025GB008597, 2025.

Zaehle, S. and Friend, A. D.: Carbon and nitrogen cycle dynamics in the O-CN land surface model: 1. Model description, site-scale evaluation, and sensitivity to parameter estimates, Global Biogeochemical Cycles, 24, doi:10.1029/2009GB003521, 2010.

Zhang, H. F., Chen, B. Z., van der Laan-Luijk, I. T., Machida, T., Matsueda, H., Sawa, Y., Fukuyama, Y., Langenfelds, R., van der Schoot, M., Xu, G., Yan, J. W., Cheng, M. L., Zhou, L. X., Tans, P. P., and Peters, W.: Estimating Asian terrestrial carbon fluxes from CONTRAIL aircraft and surface CO_2 observations for the period 2006–2010, Atmos. Chem. Phys., 14, 5807–5824, doi:10.5194/acp-14-5807-2014, 2014.

Zhang, L., Jiang, F., He, W., Wu, M., Wang, J., Ju, W., Wang, H., Zhang, Y., Sitch, S., Walker, A. P., Yue, X., Feng, S., Jia, M., and Chen, J. M.: A Robust Estimate of Continental-Scale Terrestrial Carbon Sinks Using GOSAT XCO_2 Retrievals, Geophysical Research Letters, 50, doi:10.1029/2023GL102815, 2023.

Zhang, X., Wang, Y.-P., Peng, S., Rayner, P. J., Ciais, P., Silver, J. D., Piao, S., Zhu, Z., Lu, X., and Zheng, X.: Dominant regions and drivers of the variability of the global land carbon sink across timescales, Global Change Biology, 24, 3954–3968, doi:10.1111/gcb.14275, 2018.